Laser Microwelding of Fine Wires using Femtosecond Pulses

by

Nhat Ly

A thesis
presented to the University of Waterloo
in fulfillment of the
thesis requirement for the degree of
Master of Applied Science
in
Mechanical Engineering

Waterloo, Ontario, Canada, 2014

Declaration

I hereby declare that I am the sole author of this thesis. This is a true copy of the thesis, including any required final revisions, as accepted by my examiners.

I understand that my thesis may be made electronically available to the public.

_____

Nhat Ly

Abstract

An alternative wire joining method is explored that utilizes femtosecond laser pulses directed towards the contact point of two pieces of 25-μm diameter Au bonding wires typically used in microelectronics wire bonding. The two pieces are in the form of wire loops bonded onto four terminals in a crossing pattern. *In-situ* four-wire measurement is used to measure the contact resistance at the contact point of the crossed-wires before and after femtosecond laser irradiation. A greater decrease in contact resistance correlates to a stronger joint between the crossed-wires. Broad beam laser irradiation was initially investigated to understand the effect femtosecond laser pulses had on Au microwires. Focus beam laser irradiation was utilized later to construct a parameter space. Laser parameters of pulse energy and pulse number were varied between 20 to 40 μJ and 10 to 100 pulses respectively to develop an initial process window. With a repetition rate of 1 kHz, the corresponding average power that the crossed-wires received was between 20 to 40 mW. Over 90 % of all crossed-wires samples showed drops in contact resistance ranging from 39.8 % to 83.3 %, indicating that microwelding of fine Au wire is possible with femtosecond laser pulses. Joining mechanisms are proposed for broad beam and focus beam irradiation. SEM imaging of the weld morphologies for focus beam irradiation revealed two distinct structures on the crossed-wires: a lip structure with veins resultant from molten material splash and a fringe structure resultant of an interference pattern. Cross-section analysis reveal two different modes of joining under focus beam irradiation depending on whether the laser pulses are precisely directly between the crossed-wires. A case study was done to investigate how the firing rate of the laser affects the crossed-wire joints. Focus beam laser irradiation using lower pulse numbers in high repetition showed a larger contact resistance drop than using higher pulse numbers in low repetition. The joint breaking strength of the laser welds on the crossed-wires is too low to be measured. Conclusions are drawn based on the experimental data and future work is discussed.

Acknowledgments

I wish to thank my supervisor, Dr. Michael Mayer, for his support, assistance, and advice during the duration of my Masters research. I wish to thank Dr. Norman Zhou and Dr. Joe Sanderson for allowing me to use their laser lab facilities. I wish to thank Ali Ramadhan for his tremendous efforts with setting up and maintaining the laser. Funding was also made possible by the Natural Sciences and Engineering Research Council of Canada (NSERC) and Initiative for Automotive Manufacturing Innovation (IAMI).

Table of Contents

List of Figures

List of Tables

1. Introduction

1.1 Wire Bonding Background

As of 2013, more than 90 % of all semiconductor packages were interconnected by wire bonding [1]. Wire bonds form the primary interconnections between an integrated circuit chip and the metallic lead frame in semiconductor packaging. Wire bonding is considered to be a more cost-effective and flexible interconnect technology than flip-chip interconnects. Conventional wire bonding methods utilize a combination of pressure, ultrasonic energy, time, and temperature. The most widely used wire bonding method in the microelectronics packaging industry is thermosonic ball bonding [2]. The most common material used for thermosonic ball bonding is Au for its notable mechanical properties and high reliability during testing [2]. Figure 1 shows the ESEC 3088 Wire Bonder in the Wire Bonding Lab of the University of Waterloo along with a close-up of the bondhead. Before bonding, the wire is threaded through the wire clamp and capillary. The gas nozzles provide an oxygen-free gas environment which is required for Cu wire bonding to prevent oxidation of the wire. Figure 2 illustrates the ball-wedge bonding process. Before the first bond is formed, the free end of the wire is made into a free-air-ball (FAB). FAB formation is achieved by melting the wire end using an electrical discharge to ionize the air gap. This process is called the

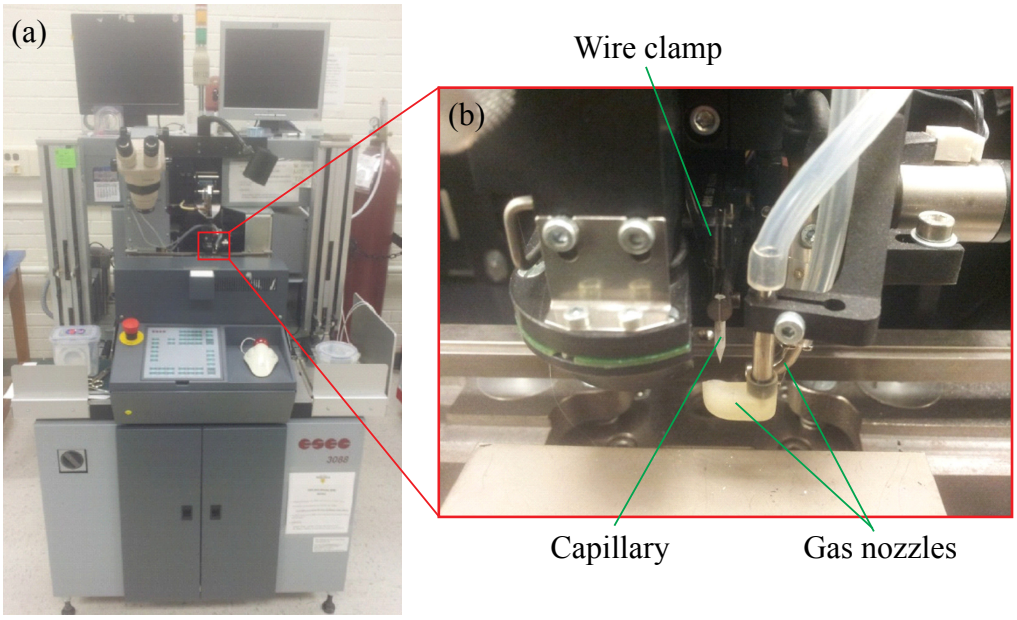

Fig. 1 (a) The ESEC 3088 Wire Bonder with (b) close up of bondhead illustrating capillary, wire clamp, and gas nozzles.

electrical-flame-off (EFO) process. During steps 1 and 2 in Figure 2, the capillary travels down to the first bond pad. The ball bond is made in step 3 by bonding the FAB to the pad using a combination of pressure, ultrasonic energy, and time. The substrate sits on top of a heater with precise control to keep the temperature of the substrate consistent. In steps 4 through 6, looping motions are programmed to obtain the desired loop height and shape. The wedge (or stitch) bond bonds the opposite end of the wire loop to the metal of the substrate in step 7 using another combination of pressure, ultrasonic energy, time, and temperature. In step 8, the capillary rises to draw the new

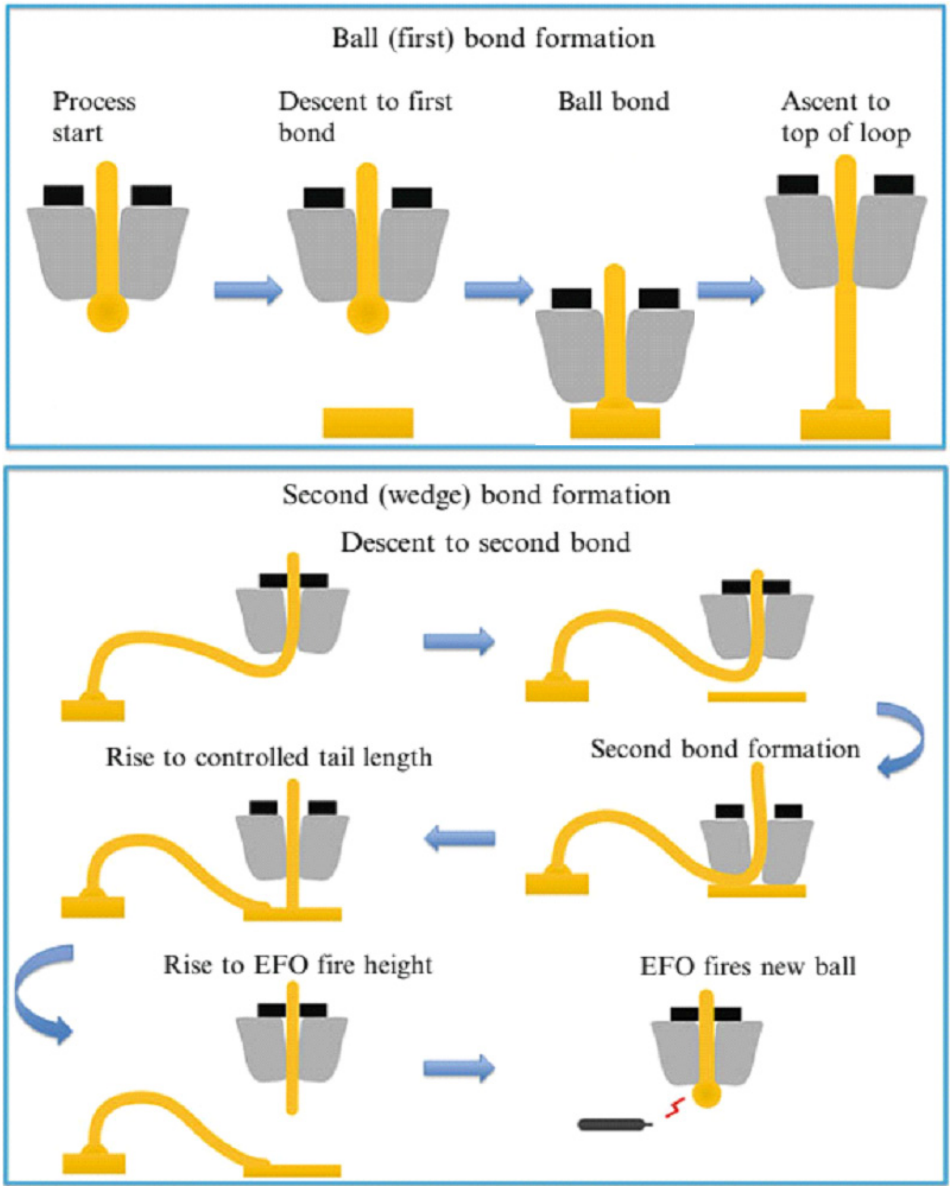

Fig. 2 The ball-wedge bond process [1].

wire tail after the second bond. The bonding tool returns to its original position for the FAB formation process in step 9. EFO firing occurs in step 10 and the new FAB is ready for the next bond cycle.

1.2 Motivation

The manufacturing of microelectronics devices with finer interconnection pitches and higher circuitry integration is a major trend in the microelectronics industry. In a review paper, Zhong et al. [3] reported various reasons why more devices require higher input/output (I/O) numbers because of the miniaturization trend. As a result, bond pad pitches are consistently being reduced in order to increase I/O numbers, resulting in many new challenges in wire bonding of ultra-fine pitch devices. Some of the challenges arise from the complex geometry of the customized designs for advanced and complex applications. A higher I/O number leads to smaller bond pad pitches which require capillary tools with smaller tip diameter.

In general, thermosonic ball bonding requires a robust substrate to withstand the high impact force and ultrasonic vibrations from the bond head as well as the high temperatures (typically upwards of 150 °C) from the heater. However, for sensitive substrates that are soft (polymers) or cannot handle the ultrasonic stresses or high temperatures, thermosonic ball bonding can be unsuitable. As the miniaturization trend introduces more complex geometry in microelectronics packages as well as more sensitive substrates, another wire joining method is worthwhile to investigate.

Furthermore, as transparent materials are fundamental to the rapidly-growing technologies of photonics, microbiology, and microanalytical chemistry, a microjoining method capable of welding wires to such materials would be useful as well [4]. A candidate for an alternative wire joining method is to use an ultrafast pulsed laser system which does not require external applications of pressure or ultrasonic energy to prevent damage to sensitive substrates. An ultrafast pulsed laser has a pulse width less than 100 picoseconds. The laser is able to introduce a high power density to a workpiece while minimizing the heat affected zone which can be favourable for complex and intricate circuit designs with high bond pad pitches. Some applications that already use a laser system for microwelding: lithium ion batteries, small size motors in various electronic devices, computer hard disks, optical fiber connectors, welding of polymers, etc. [4]. All these examples share the common theme in the sense that they are subject to the miniaturization trend, hence the

proposal to use ultrafast pulsed laser system as a microwelding tool for the low-stress and low-temperature welding of fine wires.

1.3 Thesis Organization

This work focuses on the joining of Au crossed-wires using femtosecond laser pulses. Chapter 1 gives an introduction about the thermosonic ball bonding process followed by the motivation to investigate alternative joining methods. Background review of crossed-wire welding and LMW is discussed in Chapter 2. The use of femtosecond laser pulses for the LMW of nonmetals is reviewed. Numerical feasibility studies on the joining of metals using femtosecond laser pulses were done to show that LMW of metals can be done using femtosecond laser pulses. Chapter 3 describes the crossed-wire samples, the laser setup, contact resistance measurement methods, and SEM analysis used for generating and studying the crossed-wire joints. Chapter 4 explores the use of broad beam laser irradiation for femtosecond laser joining of Au crossed-wires. Chapter 5 explores focus beam irradiation which is more applicable to micron to submicron joining. The laser parameters explored were output power and pulse number and a welding process window was summarized based on the explored parameter space. Joining mechanisms for broad and focus beam are discussed in Chapter 6. Another case study is done to determine the effect of the firing rate of the femtosecond laser. The result is presented in Chapter 7. Conclusions are drawn based on experimental results and discussion, and outlooks are given in Chapter 8.

2. Literature Review

2.1 Crossed-Wire Welding

The objective of any joining process is to produce permanent connections between parts or building blocks through the formation of primary chemical bonds between faying surfaces [2]. Over the past few decades, the product miniaturization trend has reduced the characteristic dimensions of these building blocks to the order of microns. As a result, the availability of effective microjoining processes has become one of the most critical technical prerequisites for success in manufacturing at the micron scale [2]. Microjoining can be defined as the process of joining parts that have a characteristic dimension up to 100 μm. Microjoining is essential in microelectronic packaging and interconnection. In recent years, it has evolved to encompass the manufacturing of

many miniature components, devices, and systems, such as medical implants, sensors and transducers, batteries, optoelectronics, etc. [2].

Crossed-wire welding is the joining of two wires together at an angle of approximately 90 º. One method for crossed-wire welding uses resistance spot welding (RSW). Large scale (or macro) RSW is an example of a joining method that has been studied extensively and is very well established [5, 6]. However, the process of downsizing from macro-RSW to micro-RSW is met with challenges such as electrode sticking, metal expulsion, plating issues, inconsistent electrode tip contact, and nonrepeatable welding [6, 7]. Furthermore, metals to be welded in micro-RSW are mostly non-ferrous, while the work pieces in macro-RSW are mainly steels and some aluminum alloys [7]. One application of micro-RSW is the joining of two fine wires usually at right angles with respect to each other.

The crossed-wire configuration is commonly used in electronics and instrument components, mainly for electrical interconnections [8] e.g. for use in medical devices. Fukumoto and Zhou [8] investigated the basic joining mechanisms of 0.4-mm-diameter nickel (Ni) wires, with respect to the main process parameters of welding current, welding force, and weld time. Figure 3 shows the schematic of the crossed-wire setup used in their study. The large arrows indicate the direction of the electrodes for spot welding. Through detailed mechanical testing and metallurgical examinations, the welding current and force were found to have the greatest effects on joint strength, in

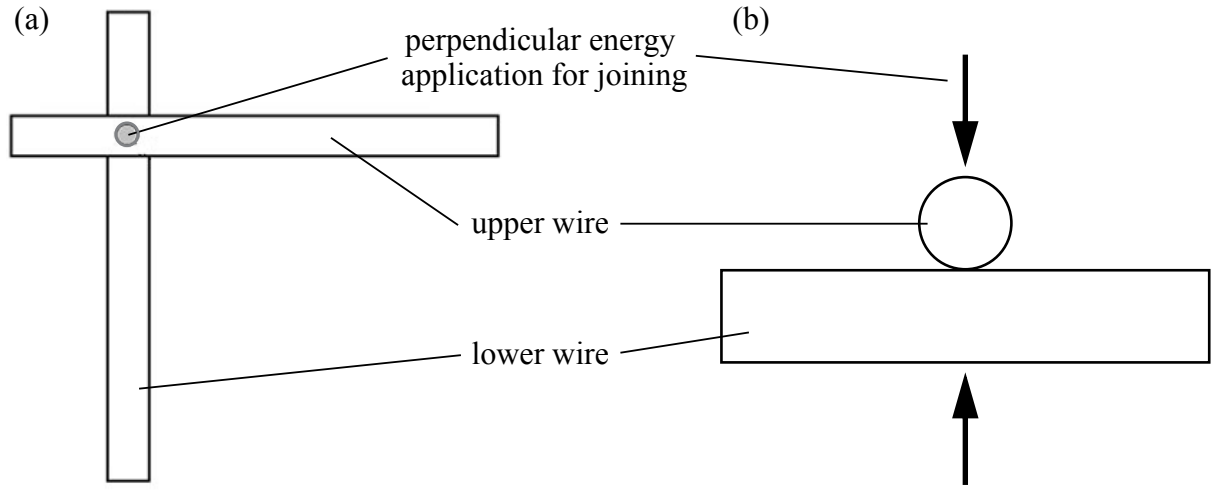

Fig. 3 Schematic of two wires crossed at right angles [8, 9]. The energy application is from the electrodes for micro-RSW as indicated by the arrows. A similar setup is later used by Zou et al. [13] and Huang et al. [14] for laser microwelding. In their studies, the energy application is from a pulsed laser and from one direction only (i.e. top arrow).

contrast to the weld time parameter. A high-quality weld for the fine Ni wires was achieved with a proper balance of high initial contact resistance and sufficiently high welding force, which could be easily realized by setting a low firing force compared to the nominal welding force [8].

In another study, Fukumoto et al. [9] investigated 0.4-mm-diameter Ni wires with a 4-μm thick Au plating. An increase in joint breaking force (JBF) was observed for the Au-plated Ni wires compared to the bare Ni wires. The formation of a fillet at the edge of Au-plated Ni joints reduces the stress concentration during tensile testing compared with the presence of a sharp notch in joints of bare Ni wires. Figure 4 shows sample optical images of the crossed-wire joints and illustrate the mechanism of joint formation during the micro-RSW of Au-plated Ni wires. Brazing is observed at low current, a combination of brazing and solid-state bonding is observed at intermediate welding current, and a mixture of solid-state bonding and fusion welding is observed at high welding current. The strength of the joint reached a peak value with increasing welding current and subsequently decreases slightly after, indicating an optimal current for the micro-RSW of fine Au-plated Ni wires.

More recently, the micro-RSW of dissimilar materials has seen a lot of attention. For medical applications, Pt alloys, such as Pt with 10 % Ir (Pt-10Ir) has been widely used for its excellent electrical conductivity, durability, biocompatibility, and oxidation resistance [2, 10, 11]. However, Pt alloys are expensive, and making complete circuits from the material is not cost effective. Hence, there is an increasing demand in the fabrication of electronic and medical devices (i.e. pacemakers, cochlear implants, etc.) for electrical connections between components of dissimilar materials in order to reduce costs. As a biocompatible metal with good mechanical strength, ductility, corrosion resistance, fabrication properties, and its availability at relatively low cost, 316 low-carbon vacuum (LVM) stainless steel is a good candidate for use in micro-RSW with Pt-10Ir [10-12]. With the 316 LVM SS wire on top, Huang et al. [11] found that the electrode force was a key factor during the welding process of dissimilar crossed-wires. Welding in low electrode force results in excellent JBF, but electrode sticking and poor surface quality were observed. In contrast, with increasing electrode force, the JBF was sacrificed due to weld defects, such as cracks and notches, but there were no electrode sticking and expulsion.

The micro-RSW of dissimilar materials, such as 316 LVM SS and Pt-10Ir has disadvantages. The desired localization of melting only at the faying interface is not possible due to the differ-

ences in electrical and thermal resistivity. As the welding current is increased, the 316 LVM SS wire with the lower melting temperature and the higher electrical resistivity melts and wets the unmolten Pt–10Ir wire [11]. Furthermore, the 316 LVM SS wire can also melt at the electrode interface which leads to electrode sticking and expulsion. In addition, softening of the 316 LVM SS wire and the round wire geometries was found to lead to the formation of notches on both the weld surfaces as shown in Figures 5(a)-(d). The softened 316 LVM SS wire is essentially cut by the Pt–Ir wire due to the force applied by the electrodes. With relatively high heat input, the mol-

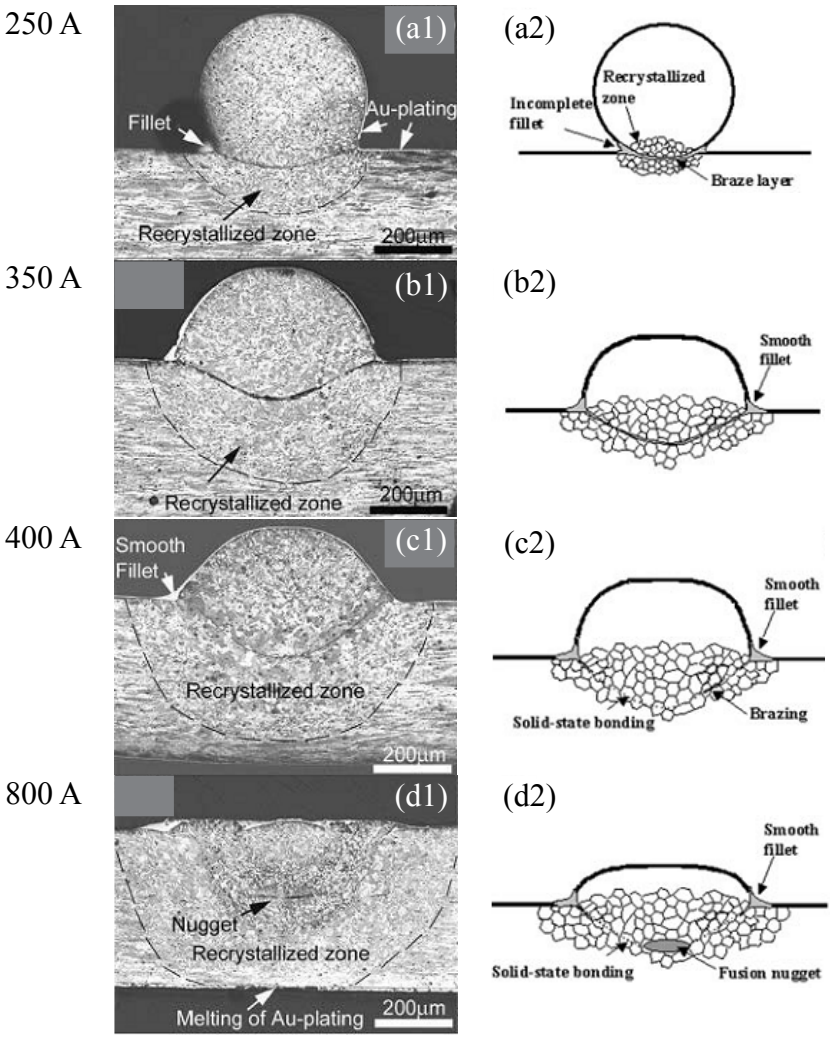

Fig. 4 Optical images (left) and schematic illustrations (right) of joint formation during micro-RSW of Au-plated Ni wires with increasing welding current showing: (a) Brazing with the formation of incomplete fillet, (b) brazing with the formation of smooth fillet, (c) combination of brazing and solid-state bonding at the interface, and (d) combination of solid-state bonding and fusion welding [9]. Welding time of 80 ms was used.

ten 316 LVM SS can heal the notch but that increases the possibility of expulsion and electrode sticking. To overcome the notch issue, a multi-pulse welding process was used to produce a sound joint with a JBF up to 87 % of the tensile strength of the Pt–10Ir wire with an acceptable surface quality as shown in Figure 5(e) [11]. With the increased complexity of medical devices, renewed challenges emerge in the micro-RSW of dissimilar biocompatible materials. Primarily, it is the difference in the materials physical properties (such as thermal and electrical resistivity) that is hindering the advancement of micro-RSW of dissimilar metals [10, 11, 13-15].

Another common joining process used for microscale fabrication is laser microwelding (LMW) [4, 12-15]. LMW offers advantages such as precision, no contact with work pieces, small HAZ, and consistent and reliable joints. Zou et al. [13] and Huang et al. [14] have investigated the LMW of 316 LVM SS and Pt-10Ir crossed-wires using an Nd:YAG laser system. Similar to the micro-RSW of Au-plated Ni, it was found that with increasing peak power, the joining mechanism transitions from brazing to a combination of brazing and fusion welding and, finally, to complete fusion welding [13]. Figure 6 shows sample optical images of the crossed-wire joints and illustrates the mechanism of joint formation during the micro-RSW of 316 LVM SS (top) and Pt-10Ir (bottom) wires. Analogous to the micro-RSW of Au-plated Ni wires, brazing was observed

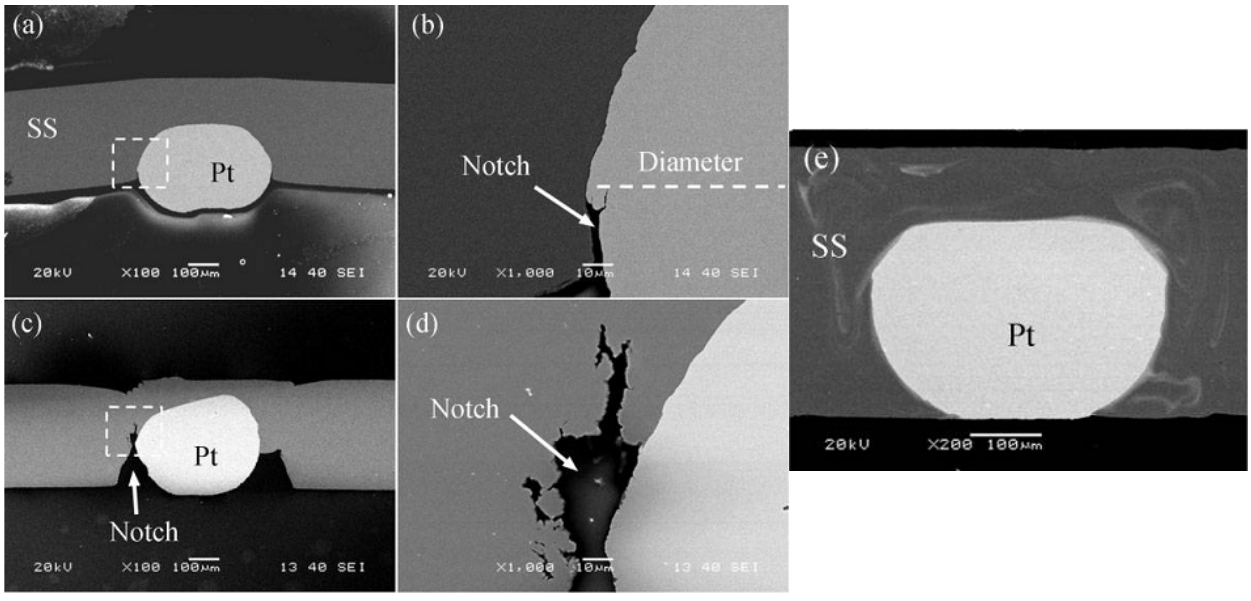

Fig. 5 Low and high magnification SEM cross-sectional images of joints welded with electrode force of 5 kgf and current of (a), (b) 300 A and (c), (d) 400 A, showing formation of notches. (e) A sample produced from the multi-pulse welding process; no notches were observed [11].

at peak powers below 0.24 kW, a combination of brazing and fusion welding was observed at within 0.25 to 0.35 kW, and complete fusion welding was seen above a peak power of 0.38 kW. LMW with peak power above 0.41 kW resulted in overwelding of the crossed-wires. Zou et al.

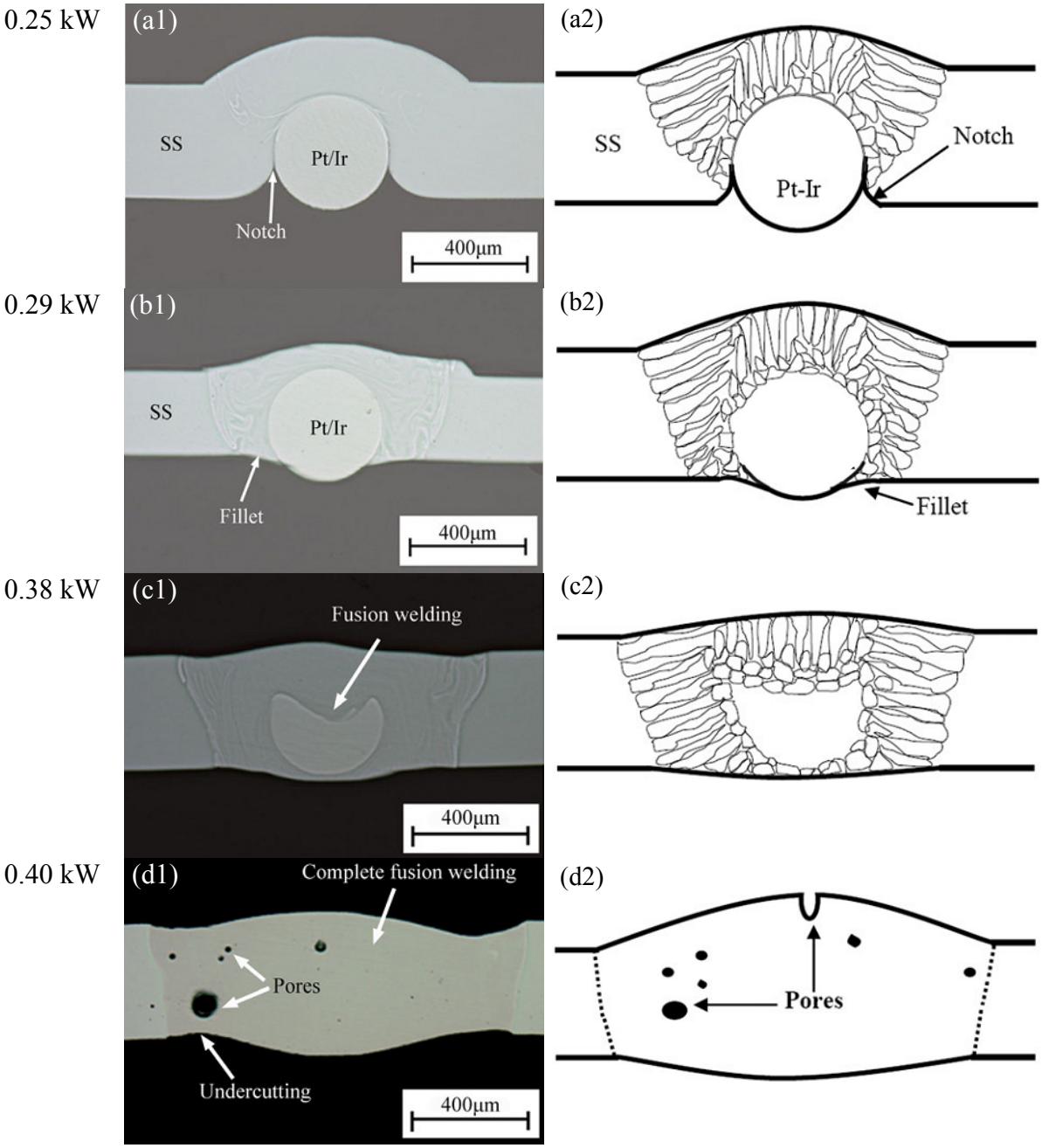

Fig. 6 Optical images (left) and schematic illustrations (right) of joint formation during LMW of 316 LVM SS and Pt-10Ir crossed-wires with increasing laser power showing: (a) brazing, (b) combination of brazing and fusion welding, (c) combination of brazing and fusion welding with complete wetting of Pt-10Ir wire, and (d) fusion welding [13].

[13] reported that the welds produced within the optimum peak power range of 0.29 to 0.38 kW had smooth surface geometry with no porosity or notches and tensile strength up to 90 % of the Pt-10Ir, resulting in the highest JBF.

In a continuation study, Huang et al. [14] concluded that the material orientation must be considered along with the temperature gradient and material properties in the laser welding of dissimilar crossed wires. The Pt-10Ir wire was subjected to the incident laser beam instead of the 316 LVM SS wire. Similar JBF values were achieved with either wire orientation. No surface pores were present, however, large pores, were found in the cross sections of the welds [14]. Figure 7 shows the cross-sections of the Pt-10Ir and 316 LVM SS welds with increase laser power. The difference in melting temperature and the resultant temperature gradient in the joint during welding caused the Pt-10Ir wire to partially melt and the 316 LVM SS wire to completely melt as the laser

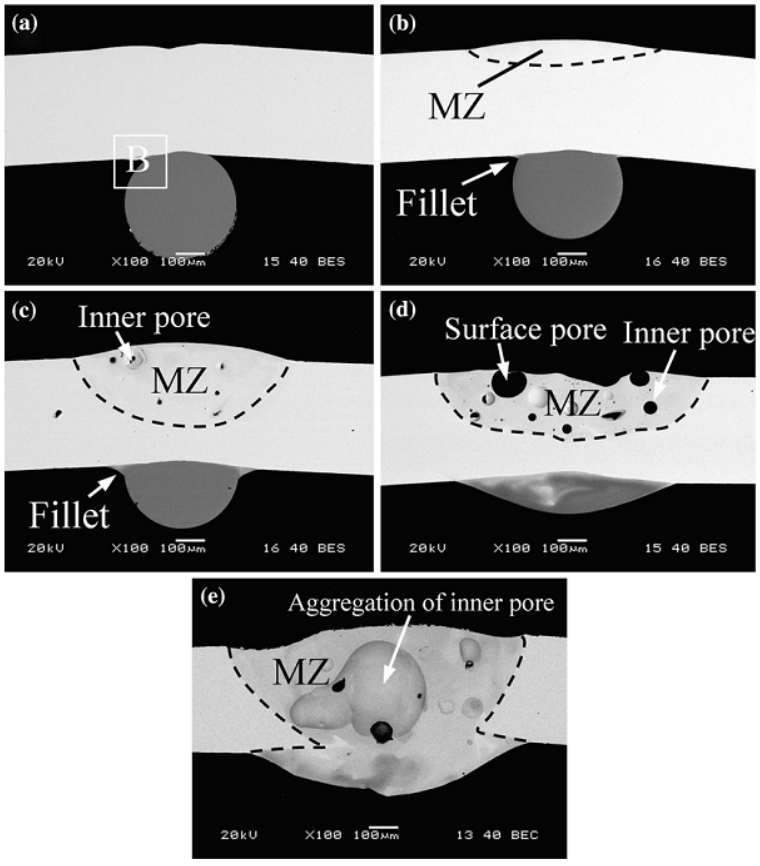

Fig. 7 SEM images of joint cross-sections along the Pt-10Ir wire axis. Weld produced with increasing peak power starting at (a) 0.28 kW, (b) 0.32 kW, (c) 0.36 kW, (d) 0.40 kW, and (e) 0.42 kW. The dashed lines highlight the mixed zone (MZ), where elements from each of the wire materials are found [14].

power increases. The two materials mixed and undesirable porosity defects were produced as a result. Thus, Huang et al. [14] concluded that acceptable LMW welds between dissimilar Pt-10Ir and 316 LVM SS wires were only possible when the 316 LVM SS wire was subject to the incident laser beam.

The current challenges with micro-RSW of dissimilar materials can be overcome by implementing LMW. Figure 8 compares the micro-RSW and LMW of 316 LVM SS with Pt-10Ir wires, showing that dissimilar materials can be joined with an optimal set of parameters while still achieving similar JBF [15]. The LMW of wires around the order of 100 μm has been well established. However, not much published work has been done for the LMW of wires under 100 μm.

Following the miniaturization trend, typical diameter values of wire bonds used in the microelectronics packaging industry are less than 25 μm. However, the focus spot size of a typical industrial Nd:YAG or CO_2 laser is around 400 μm [2, 13, 14, 16-18], which is a factor of eight higher than the crossed-wire samples of these dimensions. An alternative laser that offers higher precision, smaller spot size, and even more localized energy input possibly is more suitable for LMW of such fine wires. Therefore, a femtosecond laser system is considered as an alternative.

2.2 Femtosecond Laser as a Welding Tool

Recently, pulse lasers are considered to the one of the best tool for a variety of microscale material joining tasks due to the high precision, non-contact nature, and ability to focus and localize the intensity of the laser light into a small area [4, 19]. Laser microwelding has found numerous integral applications in the electronic, electrical, automotive, and medical industries [4]. The minia-

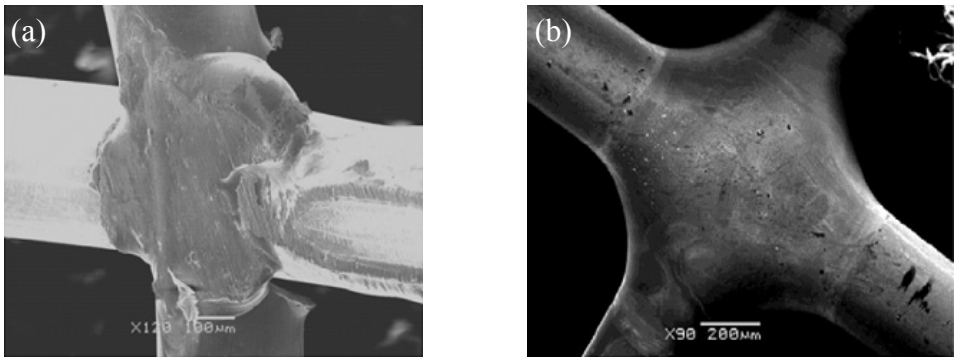

Fig. 8 (a) Excessive melting of the higher resistivity 316 LVM SS in the dissimilar RMW joint. compared to (b) LMW joint results in an acceptable weld with a smoother surface [15].

turization trend of the microelectronics packaging industry is driving laser technology to achieve beam diameters on the order of less than 100 μm. Nonetheless, laser welding of components with dimensions less than 100 μm is still a challenging task primarily due to the fact that the mechanisms for laser microwelding as such a small scale are not thoroughly understood [4, 19]. There are also many laser parameters that influence the generation of molten pools for microwelding and the amount of material remove in laser ablation. Ultrafast pulse lasers (sub-nanoseconds pulse duration) have the potential for laser microwelding of parts with dimensions of less than 100 μm.

Semak et al. [20] analytically and experimentally concluded that in order to perform microwelding at beam diameters of a few tens of microns, short pulse durations should be used. Figure 9 illustrates optical images of the fusion zones on Ni surface generated by 5 ms laser pulses with increasing output power (mJ). Theoretical models and experimental results on femtosecond, picosecond, and nanosecond laser ablation of metal targets are investigated by Chichkov et al. [21]. Very pure ablation of metal targets in vacuum with femtosecond laser pulses is demonstrated. Sharp and well defined patterns can be ablated in metal and other solid targets by an image projection technique. Preuss et al. [22] studied the ablation rates as a function of increasing fluence for non-ferrous metals at pulse duration of 0.5 ps and concluded that shorter pulses are required in order to obtain high precision and minimize thermal damage. Liu et al. [23] suggested that femtosecond pulse laser micromachining would be ideal for applications with micron and submicron feature sizes. The ablation mechanism is mainly direct vaporization of materials. Femtosecond

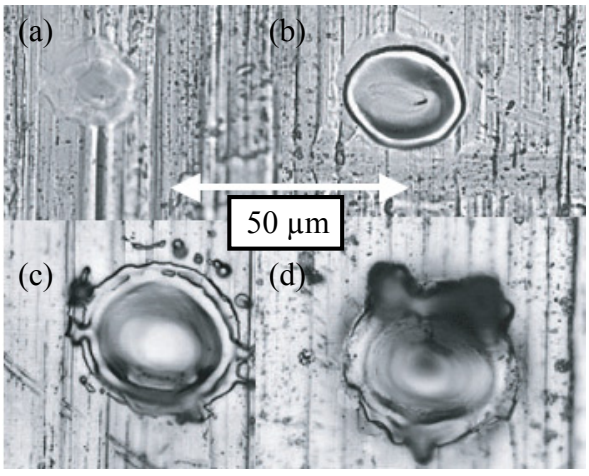

Fig. 9 Optical photos of fusion zones generated from 5 ms pulse duration as a function of increasing laser power showing transitions between (a) flat, to (b) concave, to (c)-(d) drilled [20].

lasers offer high laser intensity, precise laser-induced breakdown threshold with reduced laser fluence, and a very limited heat-affected volume. These advantages are very promising for applications in precise material processing.

For ultrashort pulses, the Two-Temperature Model (TTM) is necessary to model the laser-matter interactions due to extremely short time scale given for energy input [24]. Immediately after photoexcitation by an ultrashort laser pulse, the electrons distribute the energies among themselves via electron–electron interactions which occur over a time scale of hundreds of femtoseconds. The excited electron cloud then transfers their energies to the lattice via electron–phonon interactions. Eventually, the phonons distribute the energies to the rest of the sample through phonon–phonon interactions which also occur over a time scale of hundreds of femtoseconds. The point of significance is that the electron–electron and the phonon–phonon relaxation times are significantly shorter than the electron–phonon relaxation times because of the large difference between the electronic and lattice heat capacities [25]. The result is a state of high disequilibrium between the electrons and the lattice. Hence, it is insufficient to treat the electrons and the lattice as a whole. Instead, they are treated as two independently interacting domains: one of electrons and of phonons, each with their corresponding temperatures [24, 25]. The TTM is extensively used to model ultrafast laser spectroscopy and laser-matter interactions, especially in the submicron to nano-scale regime [25].

Many groups have investigated the use of femtosecond laser pulses for the micromachining of metals. Simon and Ihlemann [26] demonstrated submicron structuring of metal and semiconductor surfaces is possible using picosecond and femtosecond UV-laser pulses. Figure 10 illustrates a hole and periodic grating-like structures that can be created with single pulses at 248 nm on Cu.

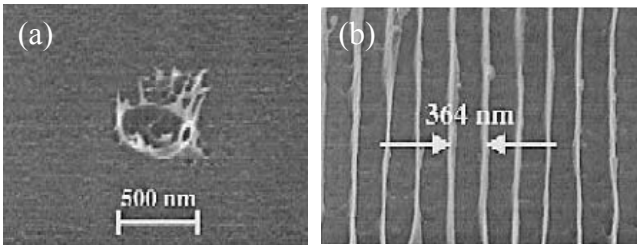

Fig. 10 (a) Hole ablated in Cu with single pulses at a fluence of 1.2 J/cm^2 and pulse duration of 160 fs. (b) Periodic structures ablated in Cu with single pulses at a fluence of 0.6 J/cm^2 at pulse duration of 500 fs [26].

The grating-like structure is generated at a fluence of 0.6 J/cm^2 with pulse duration of 500 fs. Melting of the Cu was observed at pulse duration of 160 fs and a fluence of 1.2 J/cm^2. Güdde et al. [27] and Wellershoff et al. [28] studied the energy deposition and transfer from the incident laser irradiation to the lattice of Au, Ni, and Mo [28] films of varying thicknesses. The onset of melting is defined as the damage threshold, and the threshold fluence is the input energy density required for melting. They showed that the damage threshold depends on the specific type of metal and the film thicknesses which can be well described by the TTM as shown in Figure 11. The electron-phonon coupling factor *g* also governs both the depth of energy loss into the material and the zone of thermal damage. The electron-phonon coupling factor is unique for each material. When the thickness of the material is less than the range of the coupling factor, then the fluence threshold is linearly related to the thickness, since the critical energy density required for melting remains constant [28]. Au has a higher electron-phonon coupling factor than Ni, which explains the differences between the damage thresholds as the film thickness increases. Therefore, different metallic films with varying thicknesses require different threshold fluences for submicron machining with femtosecond laser pulses.

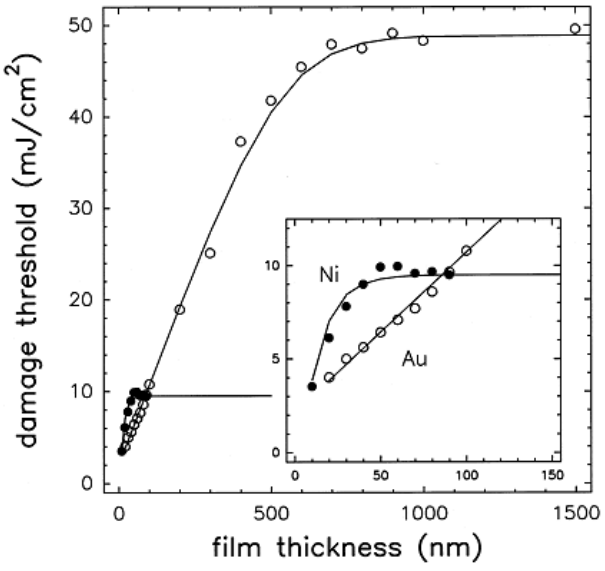

Fig. 11 Film thickness dependence of the absorbed laser fluence at the damage threshold for Au and Ni. The inset show a magnification of the thin film range. The solid lines are calculated using the TTM [27].

For bulk metallic targets (t > 100 μm), the electron-phonon coupling factor becomes a constant and the threshold fluence for melting is no longer dependent on film thickness. Momma et al. [29] and Furusawa et al. [30] investigated the ablation characteristics of thick metals exposed to femtosecond laser pulses and observed two different ablation regimes as shown in Figure 12. Momma et al. [29] initially did not conclude about the two distinct ablation regimes for their Ag target. However from Figure 12(a), the two regimes are easily distinguishable. The low to high ablation transition for Ag is estimated to be at 490 mJ/cm^2. The low and high ablation regimes for Cu are estimated to start at 93.0 mJ/cm^2 and 397 mJ/cm^2, respectively, as derived from Figure 12(b). These low and high ablation regimes can be utilized for precise laser machining of bulk metals to generate sharp, controlled submicron structures.

Femtosecond laser pulses can also be used for LMW of nonmetals. Tamaki et al. [31, 32] reported the welding of glass using femtosecond laser pulses. Figure 13 illustrates the weld morphology of the silica glass by 800-nm, 130-fs pulses at a repetition rate of 1 kHz. The interference pattern seen in Figure 13(a)-(b) is Newton's rings. The black spot under the rings indicate the substrates are in contact before and after welding. Figure 13(c)-(d) shows the cleaved surfaces of the silica glass. In a subsequent study, Tamaki et al. [32] used an amplified femtosecond Er-fiber laser system with a wavelength of 1558 nm, a pulse duration of 947 fs, and a repetition rate of 500 kHz to weld two pieces of non-alkali glass substrates, and a piece silicon substrate and to a piece of

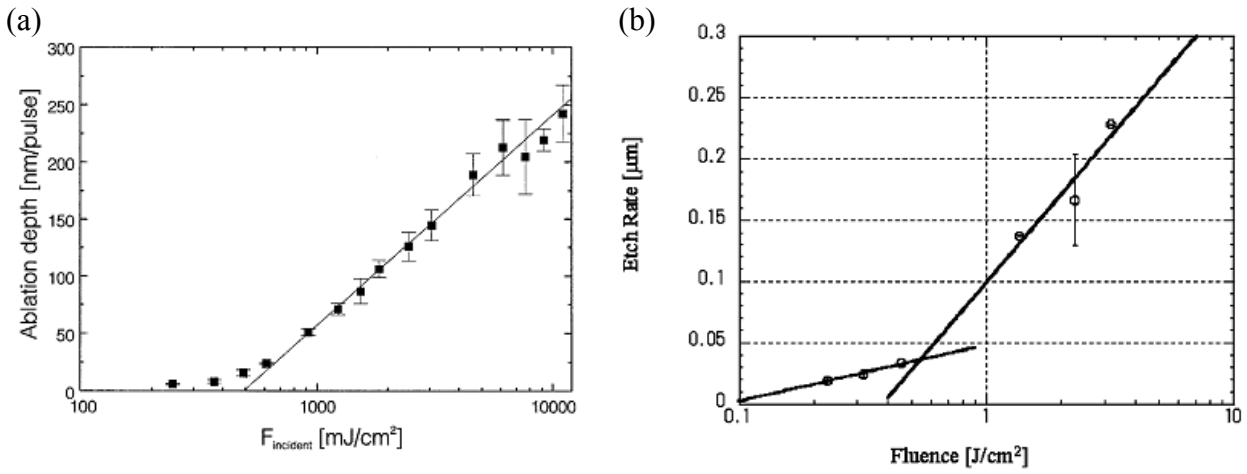

Fig. 12 The relationship between the ablation rate and laser fluence for (a) a Cu target ablated with 150-fs laser pulses at 780 nm [29] and (b) a Ag target ablated with 120-fs pulse also at 780 nm [30]. Two regimes can be observed, depending on the laser fluence.

non-alkali glass substrate. The resulting joint strength of 9.87 MPa and 3.74 MPa was measured, respectively. Ozeki et al. [33] and Sano et al. [34] successfully welded glass [33] and polyethylene terephthalate (PET) [34] to Cu using 130-fs pulses centered at 800 nm at a repetition rate of 1 kHz. Figure 14 illustrates the setup used to join Cu to glass and Cu to PET by femtosecond laser pulses along with cross-sections of the joint. The tensile strength of the Cu-to-glass joint and Cu to PET joint were > 16 MPa and 5.5 MPa, respectively. The joining mechanism between the Cu and PET is described as by Sano et al. [34] as follows. Incident ultrashort laser pulse causes local heating of Cu which results in melting and moderate ablation of the Cu in the area. The melting roughens the Cu surface and the ablation ejects the Cu nanoparticles into PET. Thermal decomposition of the material is prevented because of the extremely short temporal duration of the higher temperature state in the PET. Mechanical joining is eventually achieved between Cu and PET. Femtosecond laser direct joining of dissimilar materials (such as metals to nonmetals) shows promise as a new assembly technology of MEMS/NEMS in the field of micro-nanojoining [34].

However, there is still a lack of published work regarding the LMW of metals, primarily because the LMW of metals with femtosecond pulses is not well understood due to the complex

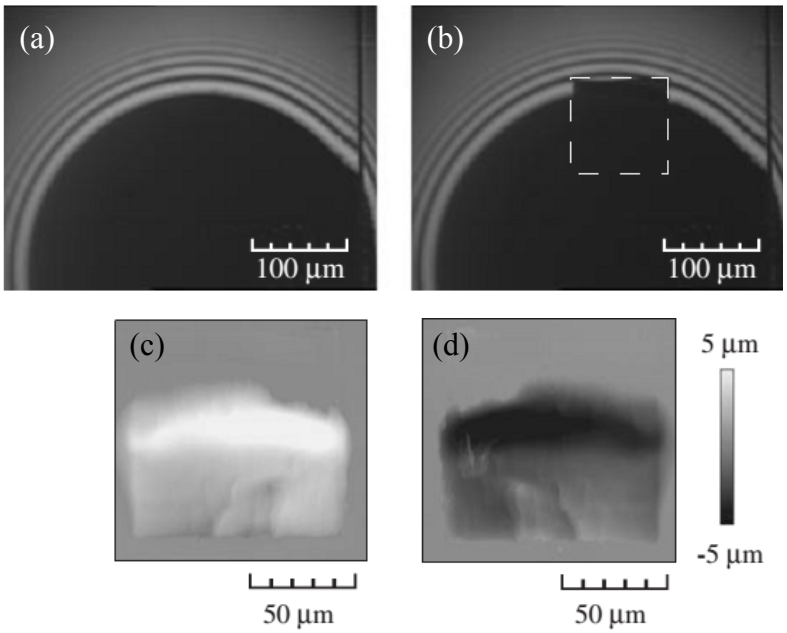

Fig. 13 Femtosecond laser welding of silica glass (a) before irradiation where Newton's rings are complete and (b) after irradiation. The white square indicates where the area of 100 µm by 100 µm in the sample irradiated with femtosecond laser pulses. (c) and (d) shows the topography of each cleaved surface mapped with the confocal laser scanning microscope [31].

nature of ultrafast laser-matter interactions. Lee [35] used the TTM to analytically determine the feasibility of LMW of Au using femtosecond laser pulses. The pictorial concept of the TTM implemented by Lee is shown in Figure 15(a) and 15(b). The three main components are the electron and lattice domains, and the interactions terms. Select laser parameters of pulse repetition rate, pulse duration, focal radius, and laser fluence for an ultrafast laser were investigated in order to understand the impact each parameter had on LMW of metals. The generalization to three-dimensions is necessary to study focal radius parameter. Figure 15(c) shows the three-dimensional dual domain configurations used by Lee. Through numerical analysis, the requirements of these select parameters for the LMW of metals with ultrafast lasers are reported as follows:

(1) low fluences with high repetition rates (1 - 10 GHz),

(2) long pulse duration (~ 100 ps) with a stable fluence, or

(3) large focal radius (> 1.0 μm) and high fluence.

The prerequisite for joining is the presence of molten material. Each of these conditions was numerically shown to maximize the depth and radius of the molten pools in the material and min-

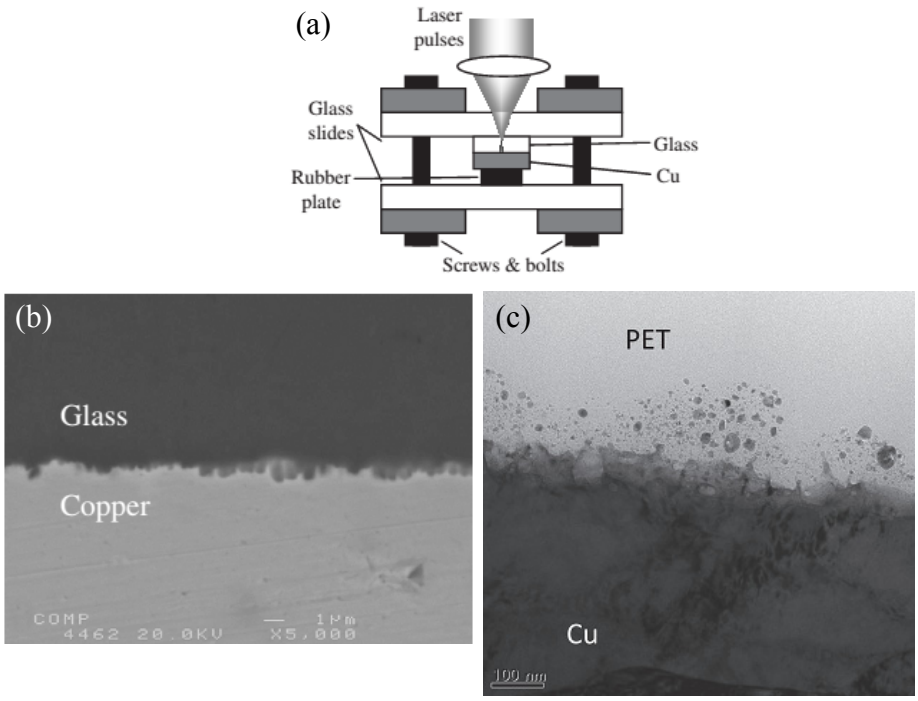

Fig. 14 (a) Experimental setup used by Ozeki et al. [33] and Sano et al. [34]. (b) SEM of cross-sectional image of laser welded Cu-glass sample by femtosecond pulses [33]. (c) TEM image of the Cu-PET joint showing the maximum strength [34].

imize the amount of material ablation. For most femtosecond laser systems, some parameters are easier to set and vary than others. In a study done by Huang et al. [36], they chose to focus on condition (3) and use a larger focal radius at high fluences. Huang et al. [36] demonstrated the joining of fine Ag wires to a Cu substrate using femtosecond laser pulses. The femtosecond laser pulses are centered at 800 nm with pulse duration of 35 fs at a repetition rate of 1 kHz. Figure 16 is the result of a weld made at a fluence of 0.08 J/cm^2 and 6000 pulses. The joining mechanism is illustrated in Figure 17. The incident laser beam ablates the nearby Cu substrate causing redeposition of Cu nanoparticles to the space between the Ag wire and Cu substrate. Resolidification of the

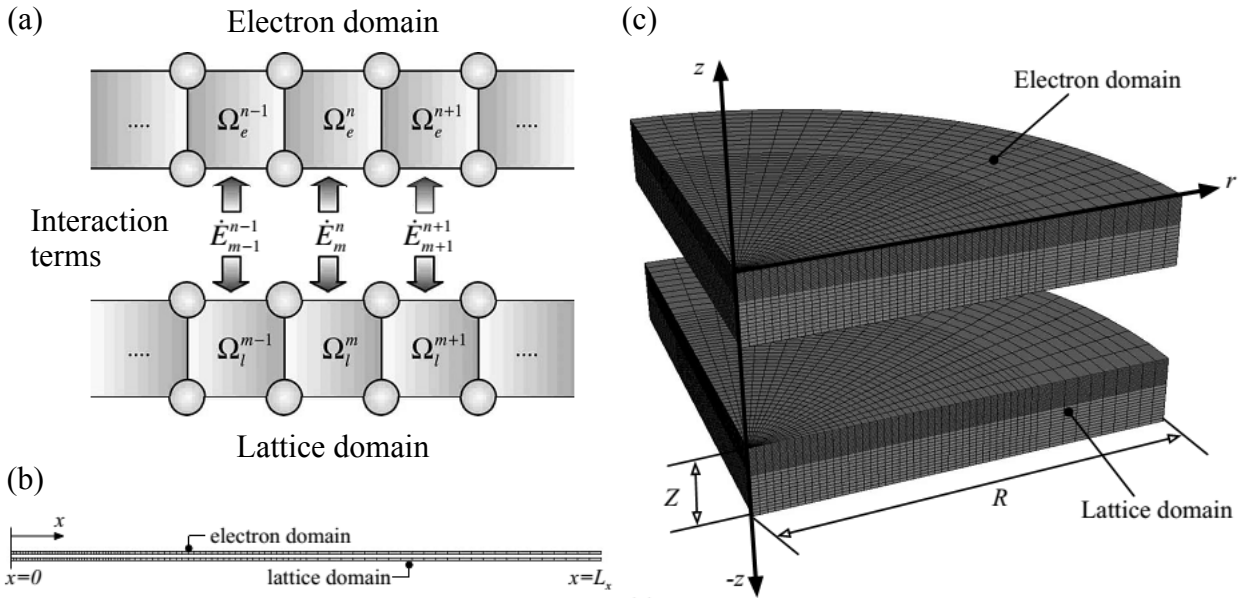

Fig. 15 (a) A section of the dual domain configuration of the TTM. The electron and lattice domains are thermally interacting with each other. The full dual domain configuration in (b) one-dimensional and (c) generalized to three-dimensions [35].

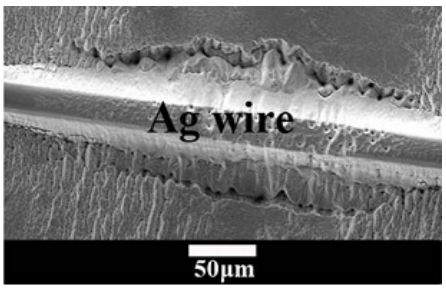

Fig. 16 Welding of 25-μm Ag wire to a Cu substrate using femtosecond laser pulses at a fluence of 0.08 J/cm^2 and 6000 pulses [36].

deposited Cu nanoparticles forms the weld "bridge" between the Ag wire and the Cu substrate [36]. The weld "bridge" is composed of three regimes: wire-to-particle welding, particle-to-particle welding, and substrate-to-particle welding as shown in Figure 17(c). The pull strength of the wires is 1.2 MPa. Such a low pull strength was attributed to the loosely welded framework and the presence of impurities in the weld. The process window to generate a successful weld is quite narrow. In a previous study, Ly et al. [37] demonstrated that the LMW of Au crossed-wires is feasible. These results will be presented and discussed in a later chapter of this thesis.

2.3 Objectives

The main objective of this thesis is to study the use of femtosecond laser pulses to weld two free-standing Au crossed-wires. The laser parameters of spot size, output power, pulse number, and firing rate are varied to develop an initial joining process and for crossed-wires joining. Weld morphologies were visually inspected via SEM imaging and contact resistance measurements were statistically analyzed to determine the quality of the weld. A process window is constructed based by the explored laser parameters. Welding models are proposed based the different welding modes observed. Cross-section methods were performed to observe the contact point of the crossed-wires in greater details in support of the proposed models.

3. Experimental Details

3.1 Crossed-Wire Samples

Commercially available 99.99 % purity 25-µm diameter Au bonding wire was used to make the crossed-wire (X-loop) samples. All wire samples are made with the ESEC 3088 wire bonder. The capillary used is an SPT capillary for 25-µm diameter bonding wire. The substrate is a ceramic

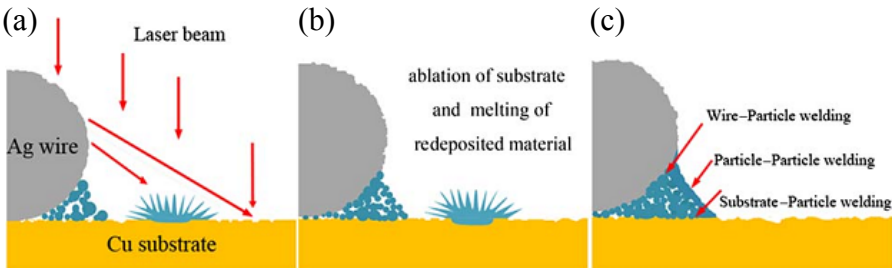

Fig. 17 Joining mechanism proposed for LMW of fine Ag wires to a Cu substrate [36].

dual in-line package (DIP) with Au metallization on the bond pads; its schematics are shown in Figure 18(a). For the X-loop samples, two 25-µm diameter Au wires are wire bonded in such a manner to ensure that they cross at one point. Figure 18(b) illustrates the layout of the X-loops on the substrate. Wire 1 and Wire 2 constitutes one X-loop sample. Following the layout, seventeen ball-wedge wire bonds are thermosonically bonded onto the Au bond pads to produced eight X-loops (Wires 1-8 and Wires 10-17) and one auxiliary bond (Wire 9). The final set bonding parameters used to generate the X-loops samples are listed in Table 1. The A typical ceramic substrate with eight X-loop samples within the central cavity is shown in Figure 18(c).

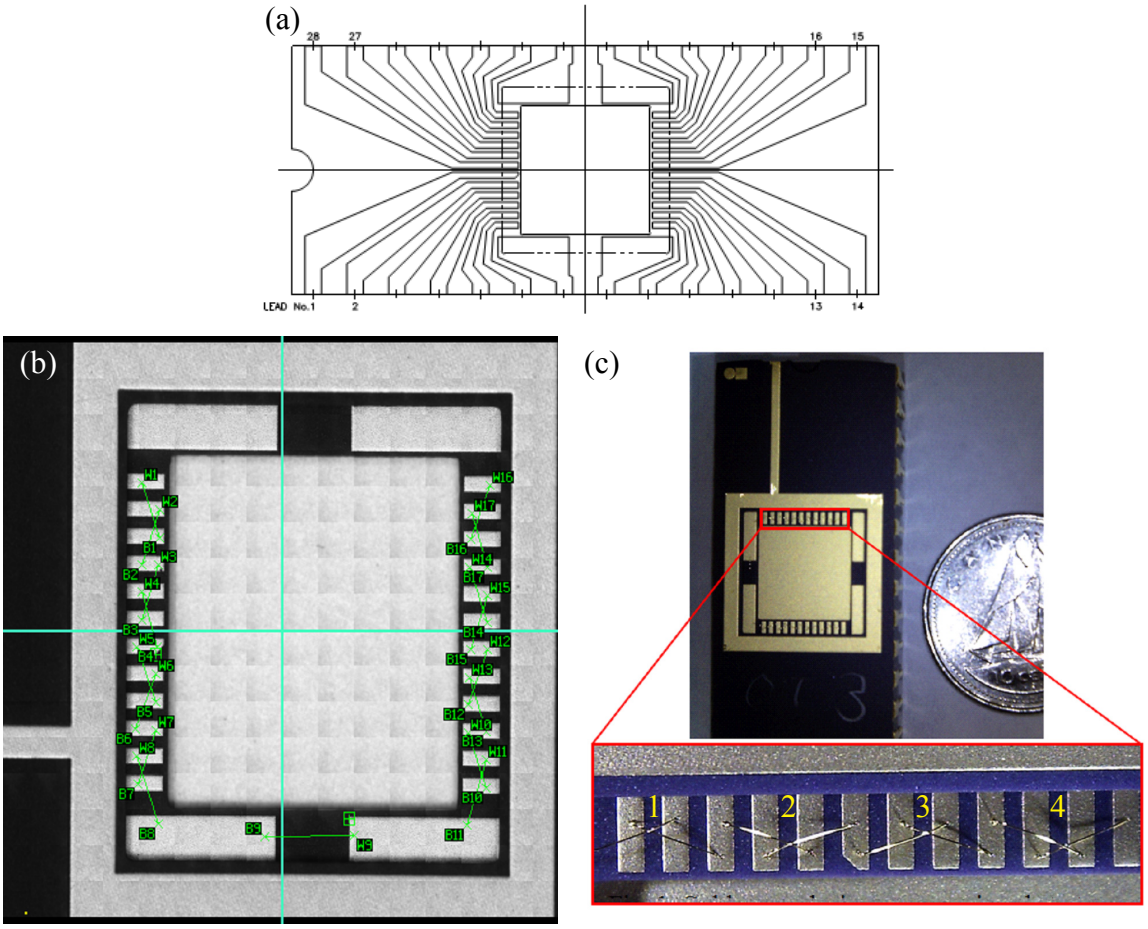

Fig. 18 (a) From Spectrum Semiconductor Materials [39], the schematic of the ceramic dual in-line package (DIP) with 28 side brazed leads. (b) Overview of X-loop layout on ceramic substrate. (c) Typical ceramic substrate with eight X-loops located in the central cavity of the DIP. The inset shows a magnified view of four X-loops.

3.2 Femtosecond Laser Setup

The initial laser pulses were produced by a Ti:Sapphire tabletop laser which are then regeneratively amplified using chirped pulse amplification [40]. Figure 19 illustrates the schematic of chirped pulse amplification. A short optical pulse is initially chirped and stretched, allowing it to be amplified to saturation while maintaining relatively low peak power. After amplification, an optical compressor is used to restore the original short pulse width, producing a resultant pulse with short duration and large energy. The outgoing laser pulse is centered at 800 nm with a fixed pulse width at a repetition rate of 1 kHz. The laser parameters investigated for X-loop joining were focus spot size (r), output power (P), and pulse number (N). The focus spot size is the radius of the surface area irradiated by the laser pulses. The focus spot size is measured on the X-loop sample by measuring the laser affect zone of the material. The focus spot size is varied by moving

Table 1: Bonding Parameters for X-loops and M-loops

ESEC 3088 Wire bonder	X-loops
Wire Diameter	25 µm
Ball Impact Force	600 mN
Ball Bond Force	200 mN
Ball Bond Time	20 ms
Ball Ultrasonic Power	30 %
Wedge Impact Force	400 mN
Wedge Bond Force	400 mN
Wedge Bond Time	20 ms
Wedge Ultrasonic Power	20 %
EFO Current	18 mA
EFO Time	3.5 ms
FAB Diameter	50 µm
Tail Length	500 µm
Electrode-to-Wire Distance (EWD)	200 µm
Loop Shape	Standard
Loop Height	400 µm
Bond Temperature	80 °C

the X-loop samples closer to the focusing lens via a translation stage. By changing the input current to the laser system, the energy per pulse was varied between 20 to 40 μJ to produce an average power between 20 to 40 mW, respectively. The pulse number (N) is controlled by a shutter. A process window was developed by setting the output power to P = 20, 30, and 40 mW, and pulse number to N = 10, 20, 40, and 100 pulses. Figure 20 shows the experiment setup used for X-loop joining. The red line indicates the direction of the incident laser beam. Femtosecond laser pulses

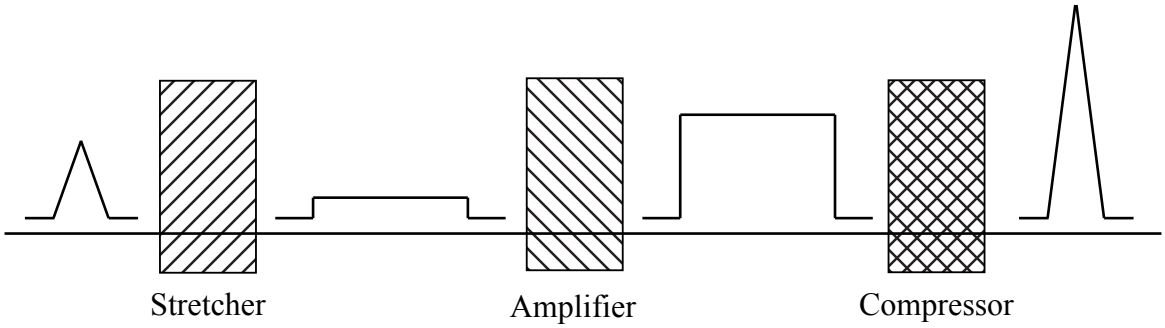

Fig. 19 Schematic of the chirped pulse amplification technique [40].

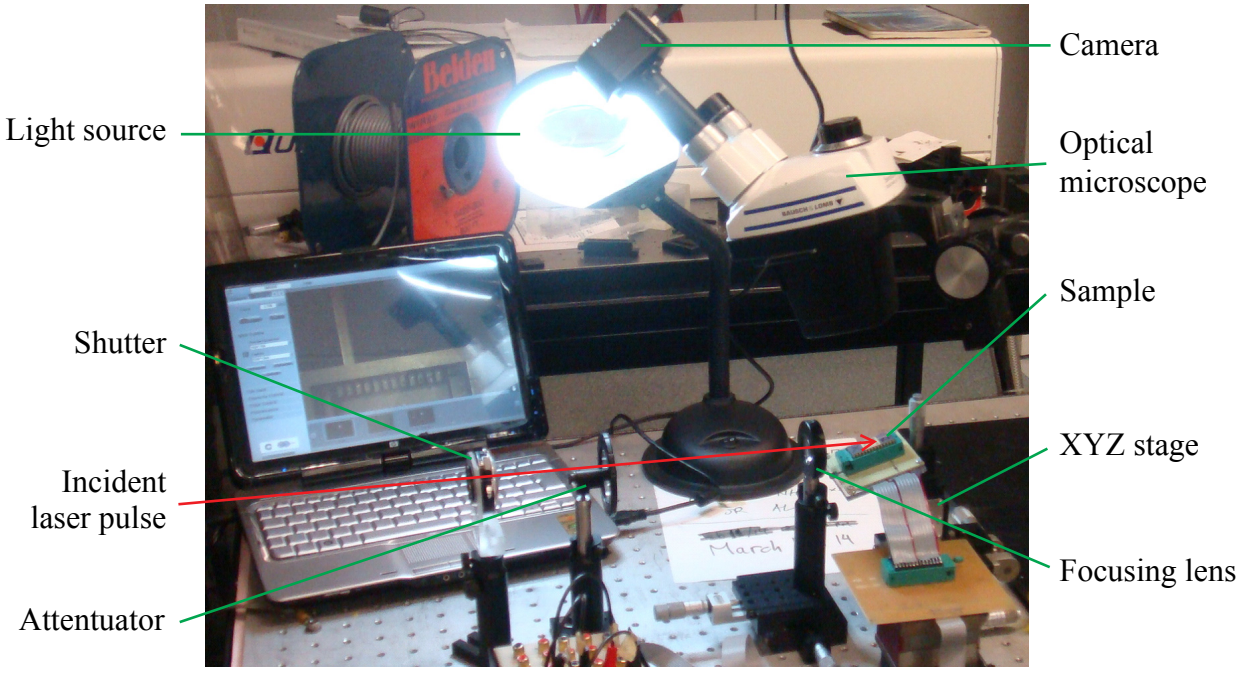

Fig. 20 Experimental setup used for laser joining of X-loop samples. The purpose of the attentuator is for aligning the laser spot with the X-loops. The sample is tilted eight degrees with respect to the horizontol to avoid clipping the laser beam.

were directed to the contact point of the X-loop samples. Because the wire bonds were produced along the rim of the central cavity of the substrate, it was necessary to tilt the substrate longitudinally to an angle eight degrees with respect to the horizontal to avoid clipping the incoming laser beam for the smaller laser spot sizes. For the larger laser spot sizes, the incoming laser irradiation is parallel to the normal of the substrate. The laser spot size is varied by adjusting the distance the sample is situated with respect to the focusing lens. The focusing lens has a focal length, *f,* of 5 cm. The smallest laser spot size achieved by the lens is 20 μm. The X-loop samples were situated on an XYZ translation stage. The attenuator was used to reduce the laser intensity so that the laser spot can be observed under microscope camera, allowing proper alignment of the laser spot to the contact point of an X-loop. A shutter was used to control the pulse number incident onto the X-loops. Once aligned, the attenuator was removed and the shutter was triggered to allow the incident pulses to pass through the focusing lens and subsequently focused onto the X-loop samples.

3.3 Four-Wire Measurement and SEM Analysis

In-situ four-wire contact resistance measurement is used to determine the quality of the weld. When a constant current is applied across the crossed wires, the contact resistance, R_c, can be calculated provided the voltage drop is measured at the point of contact. Figure 5(a) illustrates a

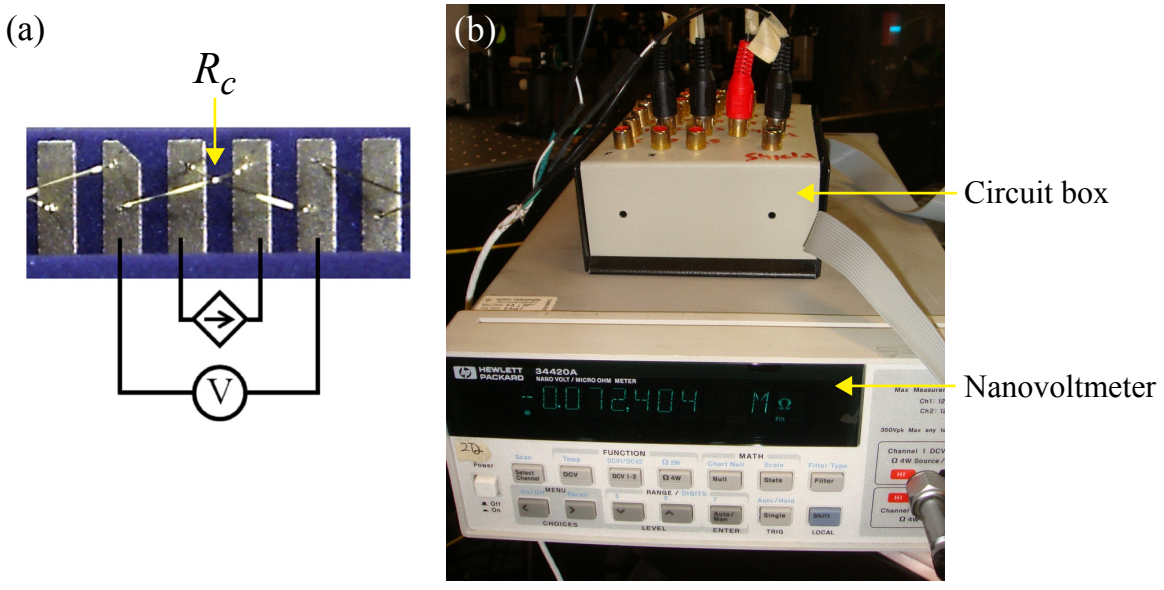

Fig. 21 (a) Schematic of the four-wire contact resistance measurement. (b) Nanovoltmeter setup for recording R_c before and after laser irradiation.

schematic of how the four terminals are set up on the substrate to measure R_c before and after laser irradiation. Knowing the applied current I and measuring the voltage drop ΔV across the X-loops, R_c was calculated using Ohm's Law. The nanovoltmeter setup shown in Figure 21(b) manages the R_c calculations as well as corrects for any offsets, and display an R_c value before and after laser irradiation. The four wires from the nanovoltmeter connect to a circuit box which provides an interface to the ribbon cable integrated into the sample holder shown in Figure 20. The bonding parameters listed in Table 1 generates X-loops with consistent initial contact resistances. After femtosecond laser irradiation, the wires join to yield drop in the contact resistance of the X-loops. A stronger joint correlates to a lower final contact resistance.

SEM imaging of all X-loop and M-loop samples was done using the Zeiss ULTRA *plus* high resolution field emission scanning electron microscope (FE-SEM) at an accelerating voltage of 20 kV. Cross-sections of the X-loops and M-loops welds were prepared using conventional metallographic techniques. The X-loops on the DIP was encapsulated in a cold mount epoxy. A precision saw equipped with a diamond studded bladed was used to cut around the DIP central cavity containing the eight X-loops. Initial manual grinding was performed using 80 grit sandpaper. Visual cues were used to determine when the cross-section of interest is almost in reach on the X-loops. Once at the cross-section, manual grinding using 1200 grit sandpaper or diamond polish was used to generate a smooth out the previous surface. A final, flat finish was achieved using ion milling on a LEICA EM TIC 3X system.

4. Broad Beam Irradiation

An SEM image of a typical X-loop sample before laser irradiation is shown in Figure 22(a). The crossed wires are held in place by tension making them insensitive to handling, small vibrations, and other minute disturbances in a typical laboratory setting. For broad beam irradiation, the X-loop samples were positioned just before the focal point of the focusing lens. The laser system used for broad beam irradiation is identical to the one used by Huang et al. [36]. The laser pulses were centered at 800 nm with a pulse duration of 35 fs at a repetition rate of 1 kHz with a maximum pulse energy of 3.5 mJ. Figures 22(b) to 22(e) show the X-loops after laser irradiation. The wires along with the bond pads lost their smooth surface morphology; the result is defined as a laser affected zone (LAZ). The laser affected zone gives information about the area of the laser

spot size. The spot size used for broad beam laser irradiation is measured to be ~ 500 μm. The surface morphology after laser irradiation is covered with squiggling vein-like structures that appear throughout the Au wires and Au bond pads within the LAZ. As the laser beam is incident onto the

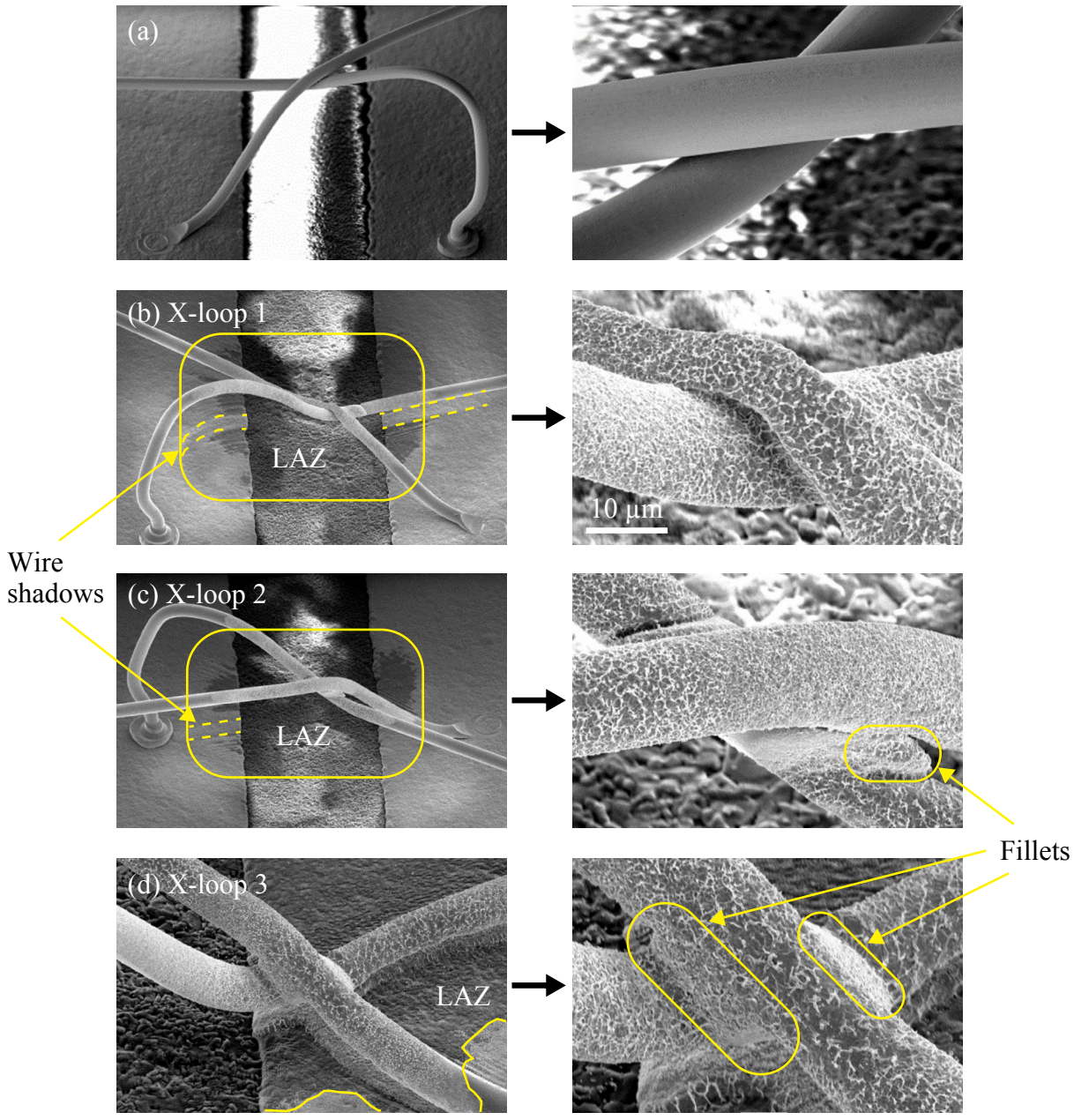

Fig. 22 (a) SEM image of an X-loop sample before laser irradiation. Left-hand side images are magnified views of the right-hand side images. (b)-(d) X-loop samples after laser irradiation at (P, N) = (1.65 W, 66 pulses). The vein-like morphology is seen everywhere within the LAZ. The focus spot size is ~ 500 μm.

X-loop, a large amount of energy is suddenly introduced onto the surface of the wires, rapidly increasing its temperature. The surface layer of Au proceeded to melt and splash around locally from the high disequilibrium. Because the laser pulse is extremely short lived, the temperature of the wires rapidly decreases and the surface of the wires resolidifies. The result are these squiggling vein-like structures showing how the molten Au is "frozen" after a state of high disequilibrium due to the ultrashort laser irradiation. The LAZs are outlined on each of the X-loop images. The wires cast a shadow over parts of the Au bond pads where the laser irradiation do not reach, keeping the bond pads' relatively smooth morphology. A fringe pattern can be seen on the Au bond pads originating from the shadow of the wires much like ripples in water after an impact from an object.

With melting of the surface of the Au wires, welding is observed between the crossed-wires. Fillets around the X-loops 2 and 3's contact point. After laser irradiation, the surrounding molten surface material of the wire accumulated into the crevices between crossed-wires due to surface tension and gravity. Resolidification of the Au material forms the fillet joint is between the crossed-wires. For X-loop 3, portions of the wires extending away from the central contact point is joined to the Au bond pad in a similar manner as the crossed-wires. The femtosecond laser pulses have exerted enough force to push this particular X-loop down to the bond pad and join the wires to the bond pad. Joining of metals using femtosecond laser pulses is evident in X-loop 3.

Contact resistance (R_c) measurements were taken for X-loops 1, 2, and 3 before ($R_{c,0}$) and after ($R_{c,f}$) femtosecond laser radiation. The R_c values are tabulated in Table 2. The two $R_{c,0}$ values show a large variation because the bonding parameters were not optimized for these X-loops. Subsequent X-loops made with the bonding parameters listed in Table 1 yield more consistent and lower $R_{c,0}$ values. X-loop 3 registered an inadmissible $R_{c,f}$ value due to the X-loop joining to the Au bond pad. The percent difference (ΔR_c%) between the initial and final R_c values are not significantly different between X-loop 1 and X-loop 2. X-loop 2 does show a lower $R_{c,f}$ value

Table 2: X-loops Contact Resistance Measurements

X-loop #	$R_{c,0}$ [mΩ]	$R_{c,f}$ [mΩ]	ΔR_c%
1	209.34	7.48	96.4 %
2	101.10	1.60	98.4 %

which can be attributed to its lower $R_{c,0}$ value compared to X-loop 1. A fillet is observed in X-loop 2 which can contribute to its lower $R_{c,f}$ value.

Using broad beam femtosecond laser irradiation, the welding is observed between the crossed-wires. The resultant joint is a fillet as shown best by X-loop 3. Broad beam laser irradiation is not suited for microjoining as the LAZ is five times greater than the characteristic length of 100 µm or less. Surrounding components within the radius of LAZ run the risk of being damaged by the lase irradiation. The next step is to use a smaller laser spot size to minimize the LAZ.

5. Focus Beam Irradiation

5.1 Weld Morphologies

For focus beam irradiation, the X-loop samples were positioned at the focal point of the focusing lens. The laser system used for focus beam irradiation is identical to the one used by Zaidi et al. [38]. The laser beam used for focus beam irradiation was centered at 800 nm with pulse duration of 100 fs at a repetition rate of 1 kHz. The focus spot size decreased to ~ 25 µm. Figure 23(a) and 23(b) shows a magnified view of the contact point of typical X-loop samples before and after focused beam femtosecond laser irradiation, respectively. A significantly smaller LAZ is observed between the crossed-wires as outlined by the red circle. The laser parameters of output power (P) and pulse number (N) used for this particular sample was (P, N) = (40 mW, 10 pulses). Approximately seventy X-loops samples were exposed to laser irradiation with varying output power and pulse number. The output laser power (P) was set to 20, 30, and 40 mW and the pulse

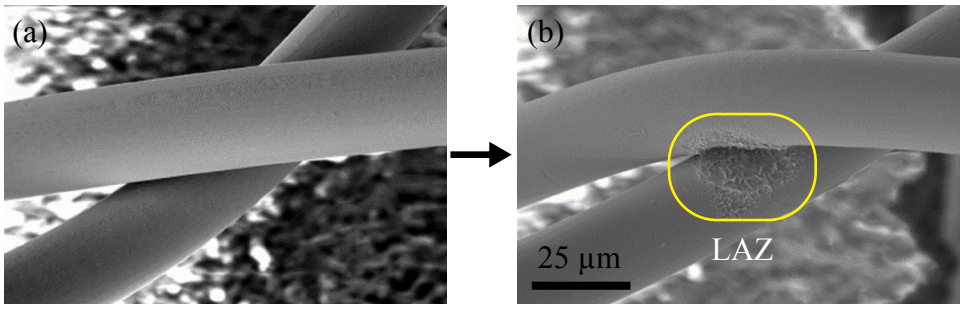

Fig. 23 SEM image of X-loop (a) before and (b) after focused beam irradiation. A smaller laser affected zone of ~ 25 µm is indicated by the yellow circle. Laser parameters used were (P, N) = (40 mW, 10 pulses).

number (N) was set to 10, 20, 40, and 100 pulses. Figure 24 shows the weld morphology for each combination of laser parameter. The smallest LAZ is less than 5 μm generated from laser parameter of (P, N) = (20 mW, 10 pulses); and the largest LAZ is approximately 25 μm generated from (P, N) = (40 mW, 100 pulses). The LAZ also shows several different structures after femtosecond laser irradiation. The most common morphology is the vein-like structures within the LAZ surrounded by a lip structure as most typically represented by (P, N) = (40 W, 10 pulses). The lip structure is the result of molten material splash as a whole. As the output power and/or pulse number increases, the lip structures are observed to be thicker and more pronounced at the edge of LAZ. This trend is expected as more energy per pulse and/or more pulses are likely to generate

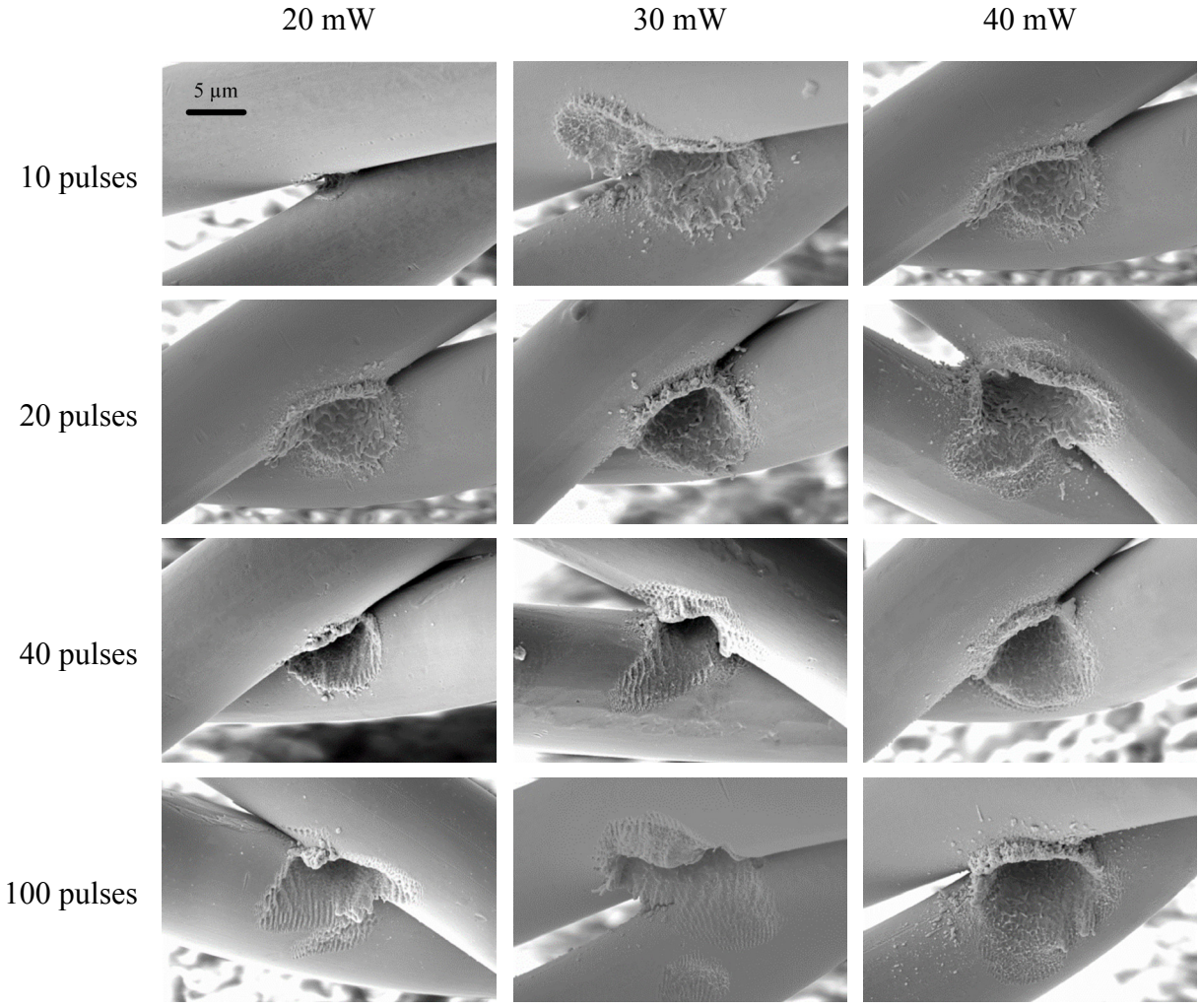

Fig. 24 Weld morphologies as a function of output power and pulse number. Increasing either laser parameter correlate to a greater LAZ at the contact point of the X-loops.

more material splash. Another distinct structure is a fringe structure as shown by (*P, N*) = (20 mW, 100 pulses). In Figure 25, the fringe pattern spacing is measured for an X-loop sample irradiated with (*P, N*) = (20 mW, 40 pulses). The measurements were made at the edge of the top wire at one particular angle. Hence, it is assumed that the fringe peak spacing remain constant along its length. The average spacing between the peaks of the fringe pattern is 1.4 µm. The fringe pattern resembles an interference pattern. However, the spacing between the fringe peaks is larger than the wavelength of the laser beam (800 nm). Assuming the fringe structure is the result of an interference pattern, this large peak spacing indicates imperfections in the laser beam during amplification or poor beam quality [40]. Furthermore, the fringe structure is only observed for (*P, N*) =

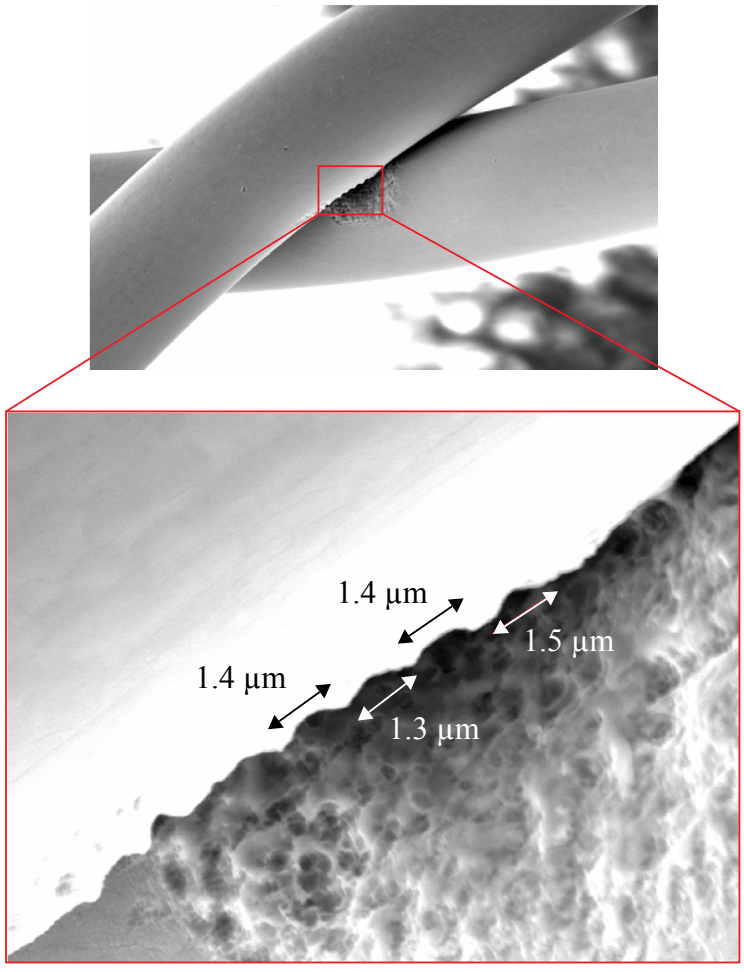

Fig. 25 X-loop sample irradiated with (*P, N*) = (20 mW, 40 pulses). The magnified view shows the fringe pattern. The average spacing is 1.4 µm. The measurements were made at the edge of the top wire at one particular angle with the assumption that the fringe spacing remains constant along its length.

(20-30 mW, 40-100 pulses), effectively encompassing the left lower quadrant of tested laser parameter space. There are also structures that show characteristics of both the lip and fringe structure as shown by (*P, N*) = (20 mW, 40 pulses).

Under constant pulse number *N*, an increase in output power from 20 to 40 mW increases the LAZ in diameter and depth. An increase in the LAZ depth with increasing laser power indicates material ablation. All samples under 40 mW have the lip structure at the edge of the LAZ. Moreover, significant debris in the form of Au droplets is observed beyond the lip structure. These Au droplets range from less than 100 nm to approximately 1.5 μm. Hence, a larger lip structure and the presence of more Au debris could be the result of more molten material splashing away from the point of impact of the femtosecond laser pulses. The observed trend is an increase in output power from 20 to 40 mW increases material ablation and generated more molten material. A similar trend is observed under constant output power and varying pulse number. The LAZ diameter increased from less than 5 μm to approximately 20 μm as pulse number increases from 10 to 100 pulses under the 20 mW. The change in LAZ diameter and depth is not as significant between 30 and 40 mW. The ideal conditions for laser microwelding are the presence of more molten material and lower material ablation. Hence, using a low pulse number between 30 to 40 mW can meet these requirements.

5.2 Contact Resistance Analysis

Statistical analysis of the four-wire contact resistance measurements were done to quantify the quality of the weld. For every combination of output power and pulse number, at least four X-loop samples were exposed to femtosecond laser irradiation. From the seventy X-loop samples made using the bonding parameters listed in Table 1, the average contact resistances was 7.61 ± 3 mΩ. More than 90 % of all samples showed a significant drop in contact resistance. The average contact resistance drops as a function of pulse number and output power is shown in Figure 26. Each contact resistance drop is calculated as a percentage difference using R_c values before and after femtosecond laser irradiation. The majority of the contact resistance drops lie between 60 and 70 %. In particular under the 30 mW setting, the contact resistance drops all fall into the 60 to 70 % range regardless of the applied pulse number.

At a constant pulse number of 10 and 20 pulses, by increasing the laser output power from 20 to 30 mW, the contact resistance drops by a significant amount. However, as the output power

continues to increase from 30 to 40 mW, the contact resistance drop is not significantly different from each other compared to the 20 to 30 mW transition. A similar case is observed for the 40 and 100 pulses. The transition from 20 to 30 mW does not result in a significant drop in contact resistance compared to the transition from 30 to 40 mW. Under the laser setting of (P, N) = (20 mW, 20 pulses), the smallest contact resistance drop of 39.8 % was observed. Under the setting of (P, N) = (40 mW, 100 pulses), the highest contact resistance drop of 83.3 % was observed. The overall trend observed is that a larger drop in contact resistance is observed as the output power and pulse number increases. For microwelding, using the (P, N) = (40 mW, 100 pulses) setting would give the best weld in terms of electrical contact.

6. Joining Mechanisms

6.1 Broad Beam Joining Mechanism

The joining mechanism for broad beam laser irradiation is similar to the mechanism proposed by Huang et al. [36] as illustrated in Figure 17. Evidence of this joining mechanism is shown in Figure 27. The femtosecond laser pulses ablate the surrounding Au bond pad. The ablated Au par-

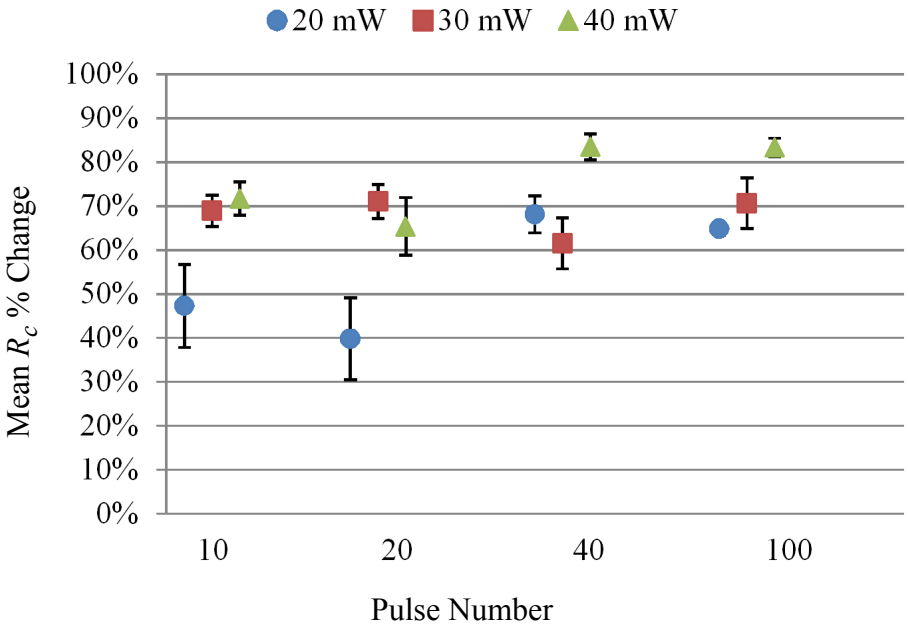

Fig. 26 Average percentage drop in contact resistance of crossed wires as a function of output power with corresponding error bars.

ticles are scattered and collected into the space between the wire and the bond pad. Even though Huang et al. [36] proposed the mechanism for wire to substrate joining, one can infer that this joining mechanism also occurs between the crossed-wires. Figure 28 illustrates a schematic of the joining mechanism for broad beam irradiation. The femtosecond laser pulses ablate and melt the surface of the wires. The molten material on the surface of the wire tends to accumulates to the space between the top and bottom wire due to gravity and surface tension. However due to the rapidly decreasing temperature of the wires after laser irradiation, not all of the molten material of the top wire make it to the bottom wire before resolidification. It is the local molten material at the point of contact that contributes the most to the joint. A combination of ablated material from the bottom wire and molten material from the top wire forms the fillets between the crossed-wires. The resultant joint resembles brazing with a complete fillet seen in the works of Fukumoto et al. [9] as shown in Figure 4(a) and (b).

6.2 Focus Beam Joining Mechanism

The proposed joining mechanism for focus beam irradiation is illustrated in Figure 29. The incoming laser irradiation is adjusted to minimize ablation but momentarily melt a thin surface

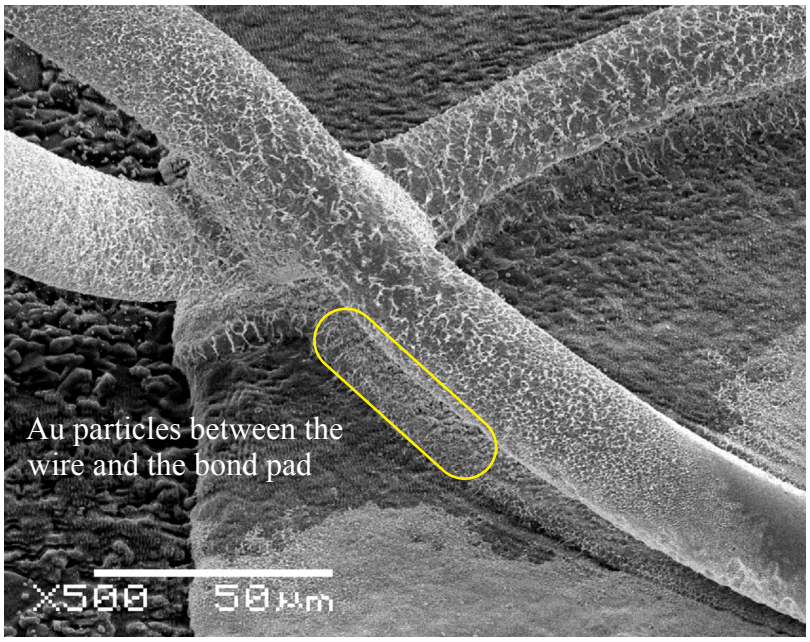

Fig. 27 Au particles deposited to the space between the wire and the bond pad as outlined by yellow circle. The fillet is composed of Au particles ablated from the surrounding bond pad. This joining mechanism was proposed by Huang et al. [36].

layer on both wires close to their contact point. After the laser irradiation, the molten material is resolidifying but not before trying to reduce surface tension by moving slightly towards the gap

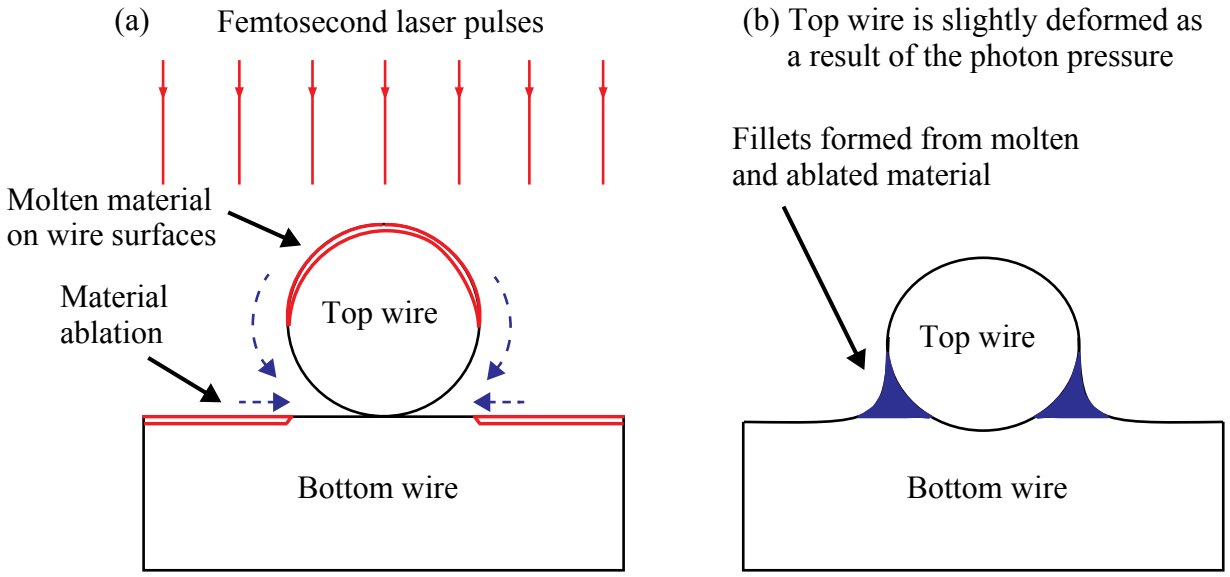

Fig. 28 Broad beam joining mechanism for the microwelding of Au crossed-wires. (a) Femtosecond laser pulses melt the exposed surfaces of the wires. The blue dashed arrows show the molten material (top wire) and the ablated material (bottom wire) travelling to the crevices between the crossed-wires due to surface tension and gravity after laser irradiation. (b) A fillet joint is formed between the crossed-wires.

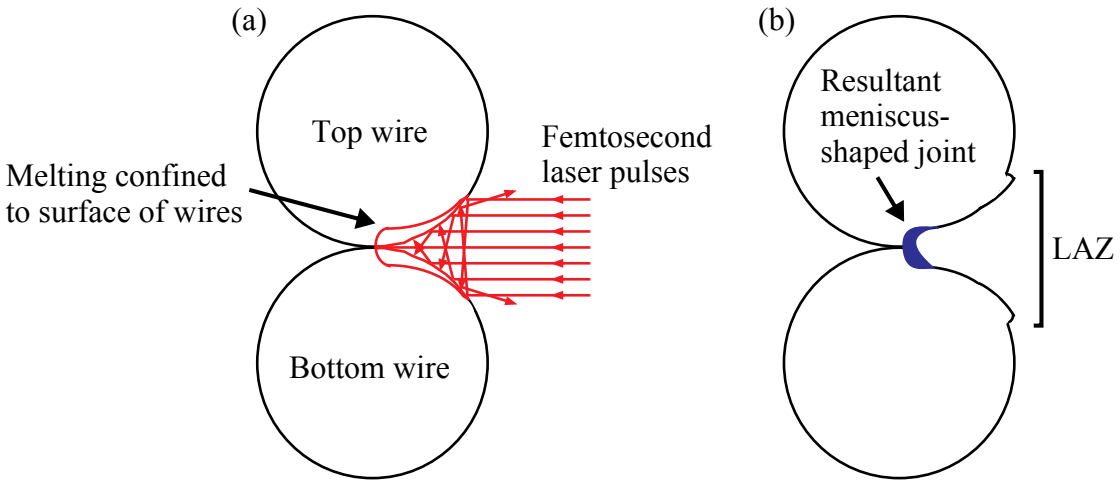

Fig. 29 Focus beam joining mechanism for the microwelding of Au crossed-wires. (a) Laser irradiation directed to contact point of X-loop. (b) Molten material remains in cavity to form the joint after femtosecond laser irradiation.

between the wires. Such pulse actions could result in the formation of a partial meniscus shaped weld metal firmly joining the two wires together. The resultant LAZ depicted is the lip structure LAZ. The diameter and depth of the LAZ increases as output power and pulse number increases. Figure 30 shows the morphology of the LAZ of the bottom wire. The dashed line represents the edge of the top wire. The morphology of the part of the LAZ highlight by the yellow circle is smoother than the rest of the LAZ. This smoothness could be evidence of the molten meniscus in the cavity of the two wires that formed the joint. Figure 31 shows the cross-sections of two X-loop samples both irradiated with laser parameters of (*P, N*) = (40 mW, 40 pulses). The laser pulse irradiated the bottom wire in X-loop A, ablating a large portion of the upper part of the bottom wire. Some of that ablated material managed to splash onto the top wire, forming a joint as result. Most of the laser energy was incident onto the bottom wire. However, some of the laser intensity arrived to the top wire as evident by the LAZ around the joint area on the top wire. X-loop B best resemble the proposed welding model. However during the encapsulation process, the crossed-wires came apart, indicating low joint strength. The magnified view of X-loop B shows the accumulated molten material that could have formed the initial weld for the crossed-wires. Both

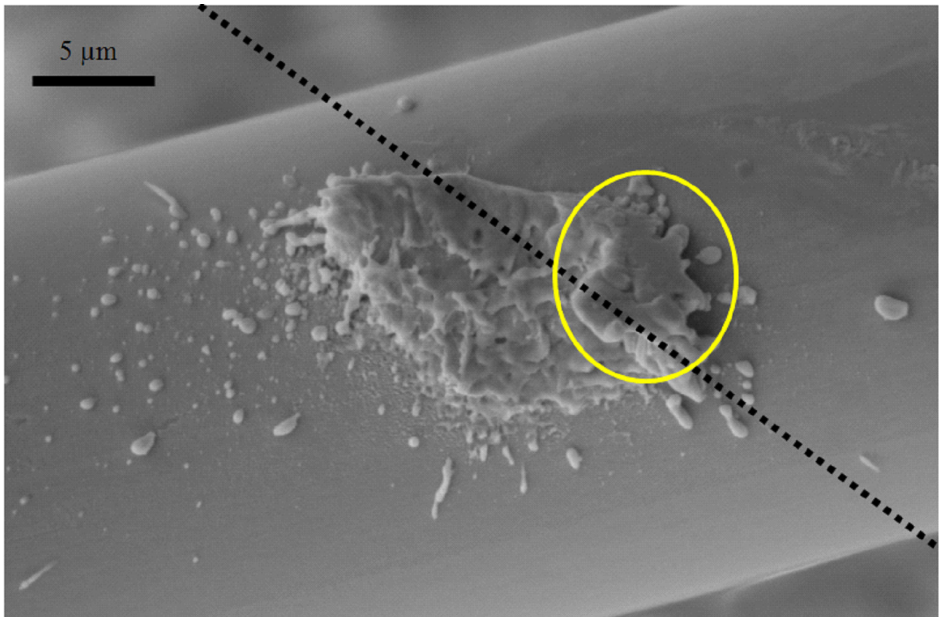

Fig. 30 The LAZ after laser irradiation with (*P, N*) = (30 mW, 20 pulses) on the bottom wire. Its length is approximately 15 µm. The proposed meniscus is shown in yellow.

X-loops in Figure 31 showed a contact resistance from of 85 %. Two welding mode is observed in the cross-sections of the X-loops. The first welding mode is seen when the laser irradiation is incident slightly off-centered from the point of contact of the X-loops. The plume of the ablated material from one wire splashes onto the other wire, forming an electrical joint. The second welding mode is if the laser irradiation is directly precisely between the two wires as proposed in Figure 29 and observed in Figure 31(b). Molten material accumulates at the cavity generated by the laser irradiation forming the joint.

7. Effect of Firing Rate

The goal of this case study was to investigate the effect the firing rate of the femtosecond laser system had on the crossed-wire samples. Using the explored process window, two laser pulse

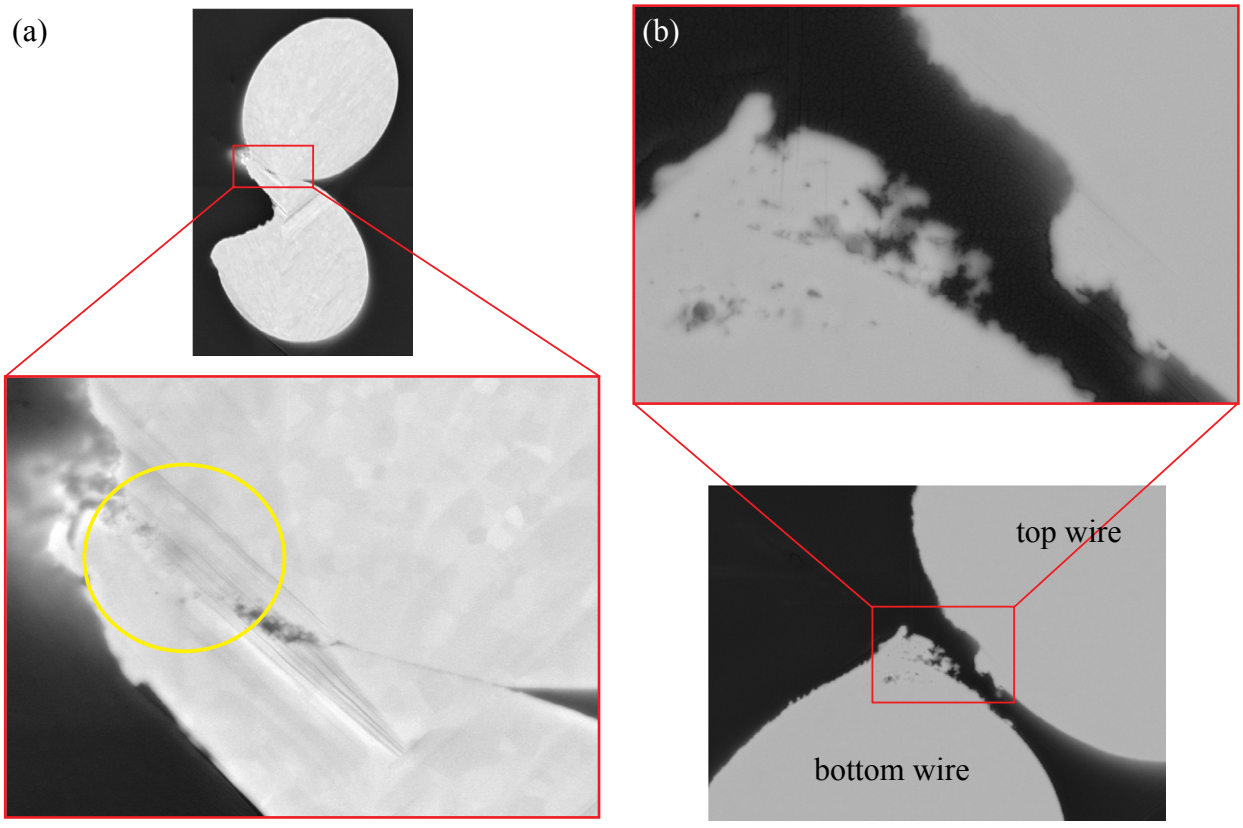

Fig. 31 Sample cross-sections of X-loops after laser irradiation with (*P, N*) = (40 mW, 40 pulses). Both samples showed a contact resistance drop of 85 % after irradiation. Welding between the bottom and top wire in (a) is highlighted in yellow.

irradiation methods were used on the X-loop samples. For both methods, 100 laser pulses were delivered to the X-loops. In Method A, the 100-pulses were delivered to the X-loops over a span of ten intervals spaced 2-3 seconds apart. In Method B, the 100-pulses were delivered in one laser shot. Recall that the shutter controls the number of pulses that is incident onto the X-loops. The number of times the shutter is triggered gives the total number of pulses. For instance, if the shutter was triggered four times, each time at the 10-pulses setting, then the total number of pulses incident on the X-loop is forty. The output power used was $P = 30 \pm 3$ mW. SEM images showing X-loops exposed to femtosecond laser irradiation using both delivery methods are shown in Figure 32. In exposing the X-loops to ten 10-pulses in succession and one 100-pulses, the observed LAZ morphologies are not significantly different between the two methods. Under Method A, the LAZs exhibit more features of the fringe structure as discussed earlier in Chapter 5 and less material splash, resulting a smaller lip structure. Under Method B, both the fringe and lip structured LAZs are observed. Furthermore, the lip structure of Method B is more pronounced than in Method A. The ten 10-pulses shots in successions generated more material splash than one 100-pulse shot. The size of the LAZs from both methods range from 20 to 25 μm in diameter.

Four-wire contact resistance measurements of the X-loops were taken for each laser irradiation method. The sample size for each method was N = 7. Figure 33 shows the average contact resistances, R_c, as a function of both laser irradiation methods. The x-axis shows the number of times the shutter was triggered resulting in the number of laser shots incident onto the X-loops. In Method A, ten consecutive 10-pulses shots were irradiated onto the X-loop samples; hence the x-axis shows ten laser shots in succession. In Method B, only one 100-pulses shot was required. The final contact resistances from both methods are not significantly different from each other. Under Method A, the first laser shot generated the largest average change in R_c, from 9.96 mΩ to 2.72 mΩ which is a drop of 72 %. Subsequent laser irradiations generated average R_c drops only up to 6 % of the initial contact resistance. The final average R_c value after ten 10-pulses laser shots is 1.38 mΩ which is drop of 86 % from the initial 9.96 mΩ. In Method B, the average R_c value started at 6.23 mΩ and dropped to 1.76 mΩ after one 100-pulses shot, which is a drop of 72 %. Method B's average R_c drop is similar to Method A's initial average R_c drop. This observation is expected as seen earlier in the explored process window shown in Figure 26. From the process

window, the average R_c drops observed from 10 pulses and 100 pulses are 69 % and 71 %, respectively. Similar or better electrical connections can be achieved through multiple irradiations of smaller pulse numbers compared to single irradiation of large pulse numbers. This can be advantageous if the targeted wire/substrate/component cannot withstand large number of laser pulses all at once. Another remarkable observation is that laser shots in succession reduce the variation of the final R_c from one sample to another. The initial R_c values vary significantly from

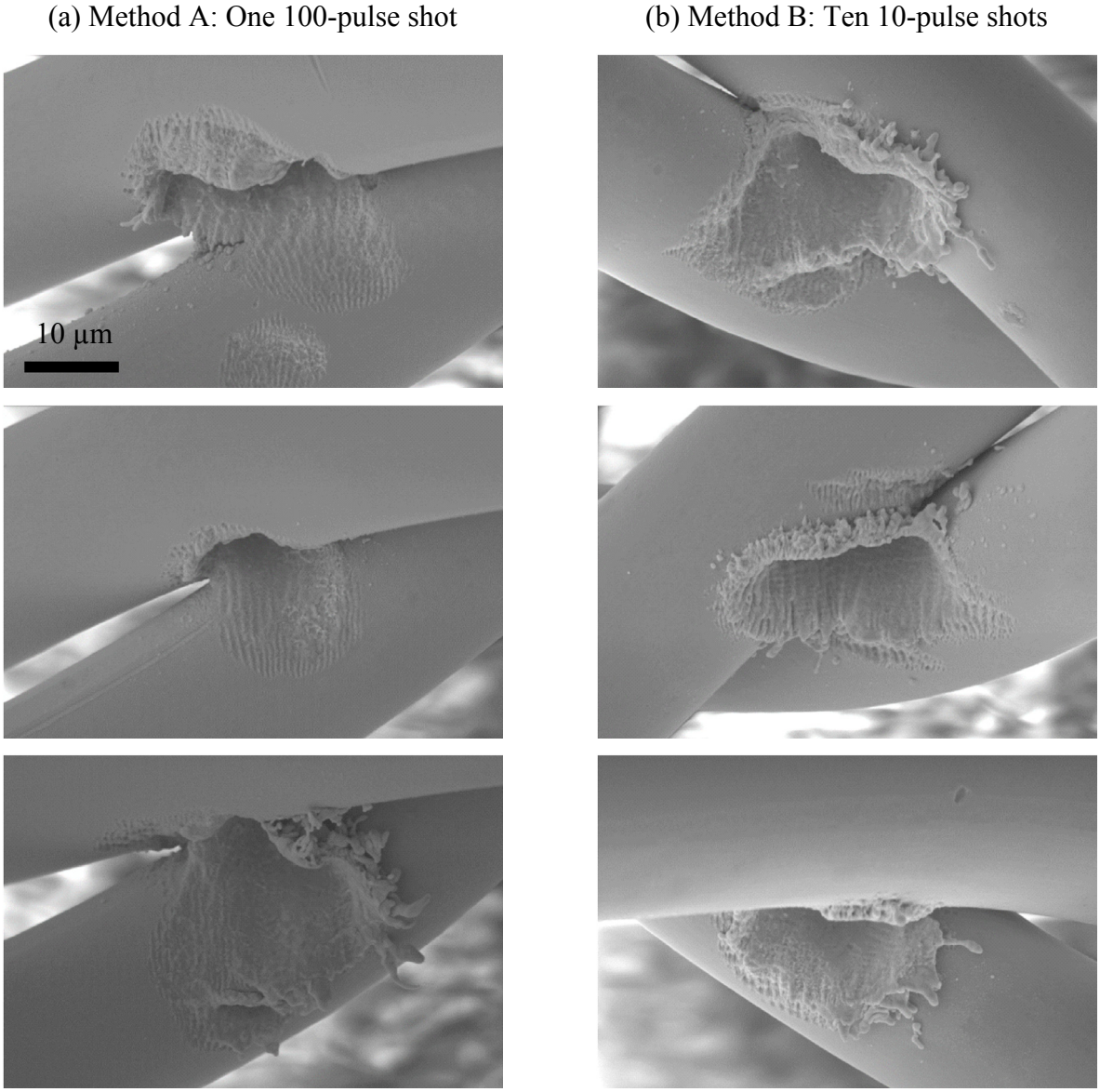

Fig. 32 SEM images of X-loops showing LAZ morphologies after femtosecond laser irradiation from (a) one 100-pulse shot and (b) ten 10-pulses shots. The fringe structure is observed under both laser irradiation methods. The lip structure is more pronounced under Method B.

one sample to another. Through femtosecond laser irradiation, the sample-to-sample variation of the R_c value decreases. In Method A, the final R_c variation is smaller compared to Method B. Having a smaller variation between the X-loop samples is advantageous for producing consistent electrical joints.

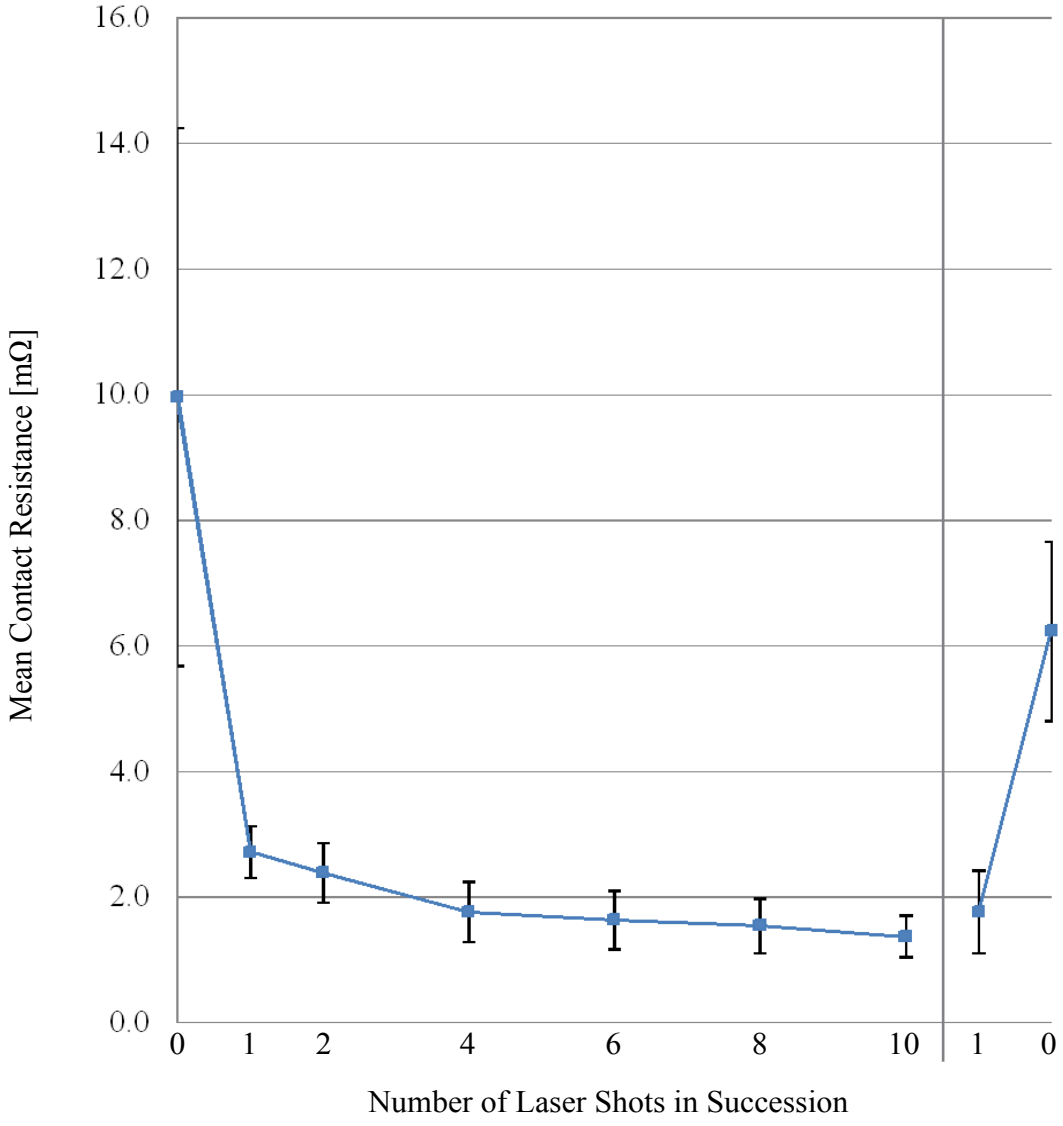

Fig. 33 Contact resistances as a function of the laser irradiation methods. The resultant contact resistance changes are not significantly different between Method A and Method B. Seven X-loop samples were used for each method.

8. Conclusions and Outlook

8.1 Conclusions

It was shown that femtosecond laser pulses can join two crossed Au microwires in air at ambient temperature without the use of additional process parameters. Broad beam and focus beam laser irradiation was investigated by varying the laser spot size. A fillet joint is observed in one of the X-loops from broad beam irradiation with an LAZ of ~ 500 µm. The morphology of the wires and bond pad within the LAZ show vein-like structures as a result of the rapid heating and cooling of the Au surface. The joining mechanism for broad beam irradiation is similar to the one described proposed by Huang et al. [36].

Since broad beam joining is not ideal for micron to submicron components, the laser spot size was decreased to ~ 25 µm. The explored parameter space was constructed by varying output power (P) and pulse number (N). The LAZ were observed to increase in diameter and depth and a greater the contact resistance drop is recorded as output power and pulse number increases. Two distinct morphologies are seen for the LAZ: a lip structure that is a result of material splash, and a fringe structure is the result of an interference pattern. The highest laser parameter setting of (P, N) = (40 mW, 100 pulses) generated a contact resistance drop of 83 %. However, for successful microwelding, the use of (P, N) = (40 mW, 10 pulses) is recommended based on this process window because of minimal ablation, which leaves more molten material for the weld.

Cross-section analysis revealed two joining modes depending on whether the laser irradiation is incident precisely at the point of contact of the X-loops or slightly towards the top or bottom wire. The preferred joining mode is to have molten material accumulate in the cavity generated by the laser irradiation to form the joint. For that, the laser irradiation needs to be precisely directly to the contact point of the X-loop. During the encapsulation process for cross-section analysis, the crossed-wires joints came apart. This indicates the JBF of the laser joints is too low to be measured by conventional pull test methods.

The effect of fire rate was investigated and conclusions were drawn based on the experimental results. In terms of the LAZ morphologies, Method B generated more molten material which results in a larger lip structure compared to Method A. Through analysis of the contact resistances, Method B generated a larger R_c drop while also reducing the R_c variation from sample to

sample. Hence, Method B is ideally better for produce more consistent electrical contacts from sample to sample.

8.2 Outlook

Broad beam irradiation demonstrated more joining characteristics compared to focus beam irradiation. The next step would be to find an optimal set of laser parameters that melts the surface of the wires similar to broad beam irradiation while minimizing the LAZ similar to focus beam irradiation. A process window can be constructed based the optimal set of parameters for the laser microwelding to two Au crossed-wires.

To expand the applications of LMW of fine wires using femtosecond laser pulses, the joining of different wire materials is worthwhile to investigate. In particular, Cu has gain much attention in the wire bonding and microelectronics packaging industry primarily due to its significantly lower cost compared to Au [1-3]. Characterizing a new process window for the joining of dissimilar metals such as Cu to Au can be another pursuit for the LMW of metals with femtosecond laser pulses. Since Ag and Al are also candidate alternate materials to Au, characterizing a process window for the joining of these materials should also be done.

Instead of crossed-wire joining, wire-to-substrate joining is also another worthwhile application for the LMW of metals. Figure 34 shows the schematics and a typical sample design for the purpose of wire-to-substrate joining. Instead of two free standing Au crossed-wires, the configuration is one Au wire in contact with a Au bond pad. These are known as M-loops. Figure 34(a) shows the M-loop geometry. The dip in the M-loop is required to make contact with a Au bond pad. Femtosecond laser irradiation will be directed to this point of contact between the wire and bond pad. A typical ceramic substrate with eight M-loop samples is shown in Figure 34(c). The other wires shown are necessary for the four-wire contact resistance measurements. The explored process window can used a starting point for M-loop joining. Once a process window is established for Au M-loops, the wire material can be switched for Cu, Ag, or Al and new process windows can be characterized. Due to geometry of the X-loops, pull tests cannot be easily performed without compromising the crossed-wire joint. Reliability testing such pull tests can be performed on M-loops.

References

[1] Chauhan P S, Choubey A, Zhong Z, and Pecht M G. (2014). *Copper wire bonding*. Springer. New York: Springer Science & Business Media.

[2] Harman G. (2010). *Wire bonding in microelectronics*. 3rd ed. New York: McGraw Hill.

[3] Zhong Z W, Tee T Y, and Luan J-E. (2007). Recent advances in wire bonding, flip chip and lead-free solder for advanced microelectronics packaging. *Microelectronics International* **24** (3): 18-26.

[4] Zhou Y. (2008). *Microjoining and nanojoining*. University of Michigan: Woodhead Publishing and Maney Publishing, on behalf of the Institute of Materials, Minerals & Mining.

[5] Tan W, Zhou Y, and Kerr H W. (2002). "Effects of Au plating on small-scale resistance spot welding of thin-sheet nickel." *Metallurgical and Materials Transactions A* **33A** August:

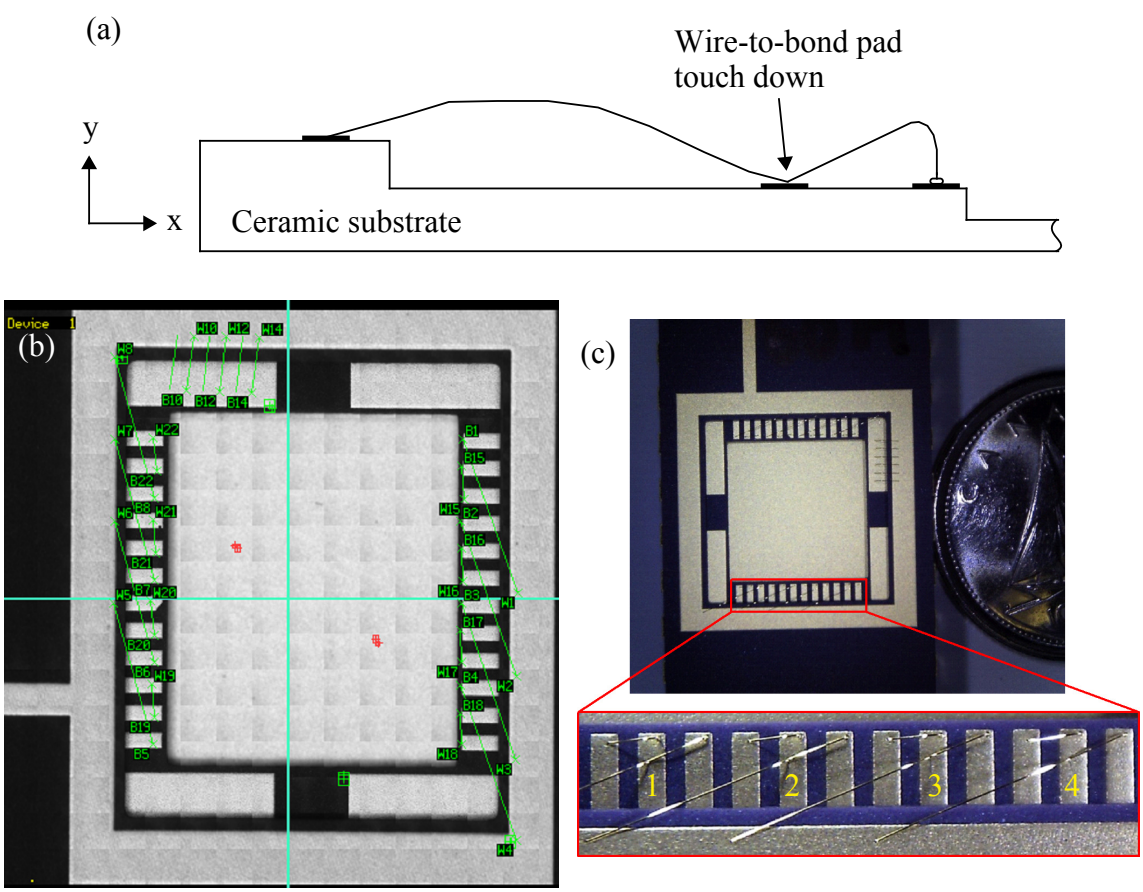

Fig. 34 (a) The M-loop geometry. The laser beam will be focused to the point where the wire touches down on the bond pad. (b) Overview of the M-loop layout on the ceramic substrate. (c) Typical ceramic substrate with eight M-loops. The inset shows a magnified view of four M-loops.

2667-76.

[6] Ely K J, and Zhou Y. (2001). “Microresistance spot welding of kovar, steel, and nickel.” *Science and Technology of Welding and Joining* **6** (2): 63-72.

[7] Steinmeier D. (1998). “"Downsizing" in the world of resistance welding.” *Welding Journal* **77** : 39-47.

[8] Fukumoto S, and Zhou Y. (2004). “Mechanism of resistance microwelding of crossed fine nickel wires.” *Metallurgical and Materials Transactions A* **35A** October: 3165-76.

[9] Fukumoto S, Chen Z, and Zhou Y. 2005. “Interfacial phenomena and joint strength in resistance microwelding of crossed Au-plated Ni wires.” *Metallurgical and Materials Transactions A* **36A** October: 2717-4.

[10] Chen Z. (2007). “Joint formation mechanism and strength in resistance microwelding of 316L stainless steel to pt wire.” *Journal of Materials Science* **42** (14): 5756-65.

[11] Huang Y D, Pequegnat A, Feng J C, Khan M I, and Zhou Y. (2011). “Resistance microwelding of crossed Pt–10Ir and 316 LVM stainless steel wires.” *Science and Technology of Welding and Joining* **16** (7): 648-56.

[12] Singh R, and Dahotre N B. (2005). “Tribology of laser modified surface of stainless steel in physiological solution.” *Journal of Materials Science* **40** (21): 5619-26.

[13] Zou G S, Huang Y D, Pequegnat A, Li X G, Khan M I, and Zhou Y. (2012). “Crossed-wire laser microwelding of pt-10 pct ir to 316 low-carbon vacuum melted stainless steel: Part I. mechanism of joint formation.” *Metallurgical and Materials Transactions A* **43A** April: 1223-33.

[14] Huang Y D, Pequegnat A, Zou G S, Feng J C, Khan M I, and Zhou Y. (2012). “Crossed-wire laser microwelding of pt-10 pct ir to 316 LVM stainless steel: Part II. effect of orientation on joining mechanism.” *Metallurgical and Materials Transactions A* **43A** April: 1234-43.

[15] Zhou Y, Hu A, Khan M I, Wu W, Tam B, and Yavuz M. (2009). “Recent progress in micro and nano-joining.” *Journal of Physics: Conference Series* **165**.

[16] Ogata Y, Takatugu M, Kunimasa T, Uenishi K, and Kobayashi K F. (2004). “Tensile strength and pseudo-elasticity of YAG laser spot melted ti-ni shape memory alloy wires.” *Materials Transactions* **45** (4): 1070-6.

[17] Gugel H, Schuermann A, and Theisen W. (2008). “Laser welding of NiTi wires.” *Materials Science and Engineering A* **481-482** May: 668-71.

[18] Tam B, Khan M I, and Zhou Y. 2011. “Mechanical and functional properties of laser-welded Ti-55.8 wt pct Ni Nitinol wires.” *Metallurgical and Materials Transactions A* **42A** August: 2166.

[19] Duley W W. (1999). *Laser welding*. New York: Wiley.

[20] Semak V V, Knorovsky G A, and MacCallum D O. (2003). “On the possibility of microwelding with laser beams.” *Journal of Physics D: Applied Physics* **36**: 2170-4.

[21] Chichkov B N, Momma C, Nolte S, von Alvensleben F, and Tünnermann A. (1996). “Femtosecond, picosecond and nanosecond laser ablation of solids.” *Applied Physics A: Materials Science & Processing* **63** : 109-15.

[22] Preuss S, and Stuke M. Demchuk A. (1995). “Sub-picosecond UV laser ablation of metals.” *Applied Physics A: Materials Science & Processing* **61** : 33-7.

[23] Liu X, Du D, and Mourou G. (1997). “Laser ablation and micromachining with ultrashort laser pulses.” *IEEE Journal of Quantum Electronics* **33** (10): 1706-16.

[24] Anisimov S I, Kapeliovich B L, and Perel'man T L. (1974). “Electron emission from metal surfaces exposed to ultrashort laser pulses.” *Soviet Physics - JETP* **39** (2): 375-7.

[25] Singh N. (2010). “Two-temperature model of nonequilibrium electron relaxation: A review.” *International Journal of Modern Physics B* **24** (9): 1141-58.

[26] Simon P, and Ihlemann J. (1997). “Ablation of submicron structures on metals and semiconductors by femtosecond UV-laser pulses.” *Applied Surface Science* **109-110**: 25-9.

[27] Güdde J, Hohlfeld J, Muller J G, and Matthias E. (1998). “Damage threshold dependence on electron–phonon coupling in Au and Ni films.” *Applied Surface Science* **127-129**: 40-5.

[28] Wellershoff S S, Hohlfeld J, Güdde J, and Matthias E. (1999). “The role of electron–phonon coupling in femtosecond laser damage of metals.” *Applied Physics A: Materials Science & Processing* **69** [Supplement]: S99-S107.

[29] Momma C, Nolte S, Chichkov B N, von Alvensleben F, and Tünnermann A. (1997). “Precise laser ablation with ultrashort pulses.” *Applied Surface Science* **109-110**: 15-9.

[30] Furusawa K, Takahashi K, Kumagai H, Midorikawa K, and Obara M. (1999). “Ablation

characteristics of Au, Ag, and Cu metals using a femtosecond Ti:Sapphire laser." *Applied Physics A: Materials Science & Processing* **69** [Supplement]: S359-66.

[31] Tamaki T, Watanabe W, Nishii J, and Itoh K. (2005). "Welding of transparent materials using femtosecond laser pulses." *Japanese Journal of Applied Physics* **44** (22): L687-9.

[32] Tamaki T, Watanabe W, and Itoh K. (2006). "Laser micro-welding of transparent materials by a localized heat accumulation effect using a femtosecond fiber laser at 1558 nm." *Optics Express* **14** (22): 10460-648.

[33] Ozeki Y, Inoue T, Tamaki T, Yamaguchi H, Onda S, Watanabe W, Sano T, Nishiuchi S, Hirose A, and Itoh K. (2008). "Direct welding between copper and glass substrates with femtosecond laser pulses." *Applied Physics Express* **1**.

[34] Sano T, Iwasaki S, Ozeki Y, Itoh K, and Hirose A. (2013). "Femtosecond laser direct joining of copper with polyethylene terephthalate." *Materials Transactions* **54** (6): 926-30.

[35] Lee D, and Kannatey-Asibu E. (2008). "Numerical analysis on the feasibility of laser microwelding of metals by femtosecond laser pulses using ABAQUS." *Journal of Manufacturing Science and Engineering* **130**.

[36] Huang H, Hu A, Peng P, Duley W W, and Zhou Y. (2013). "Femtosecond laser-induced microwelding of silver and copper." *Applied Optics* **52** (6): 1211-7.

[37] Ly N, Mayer M, Ramadhan A, and Sanderson J. (2014). "Welding of au microwires by femtosecond laser irradiation." *Paper presented at 14th IEEE International Conference on Nanotechnology*, Toronto, Ontario.

[38] Zaidi A A, Hu A, Wesolowski M J, Fu X, Sanderson J H, Zhou Y, and Duley W W. (2010). "Time of flight mass spectrometry of polyyne formation in the irradiation of liquid alkanes with femtosecond laser pulses." *Carbon* **48** (9): 2517-20.

[39] Spectrum Semiconductor Materials, Inc. "SSM P/N: CSB02825." [database online]. [cited 31/07 2014]. Available from http://www.spectrum-semi.com/products/private/drawings/CSB02825.pdf.

[40] Sugioka K, Muenier M, and Piqué A, eds. (2010). *Laser precision microfabrication*. Springer Series in Materials Science., eds. Hull R, Jagadish C, Osgood R M Jr, Parisi J, Wang Z, and Warlimont H. Vol. **135**. London, New York: Springer.